
Article:
Hasanali, M., Mojtabaei, S.M. orcid.org/0000-0002-4876-4857, Hajirasouliha, I. orcid.org/0000-0003-2597-8200 et al. (2 more authors) (2023) More accurate design equations for cold-formed steel members subjected to combined axial compressive load and bending. Thin-Walled Structures, 185. 110588. ISSN: 0263-8231

https://doi.org/10.1016/j.tws.2023.110588

Thin-Walled Structures 185 (2023) 110588

Contents lists available at ScienceDirect

Thin-Walled Structures

journal homepage: www.elsevier.com/locate/tws

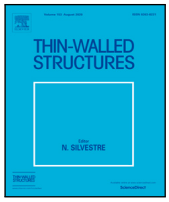

Full length article

More accurate design equations for cold-formed steel members subjected to combined axial compressive load and bending

Maryam Hasanali [a], Seyed Mohammad Mojtabaei [b,*], Iman Hajirasouliha [c], G. Charles Clifton [a], James B.P. Lim [a,d]

[a] Department of Civil and Environmental Engineering, The University of Auckland, New Zealand
[b] College of Engineering and Physical Sciences, Aston University, Birmingham B4 7ET, UK
[c] Department of Civil and Structural Engineering, The University of Sheffield, Sheffield, UK
[d] School of Engineering, The University of Waikato, Hamilton, New Zealand

ARTICLE INFO

Keywords:
Cold-formed steel (CFS)
Beam–columns
Finite element (FE) model
Interaction equation
Reliability analysis

ABSTRACT

Cold-formed steel (CFS) load-bearing members in multi-storey frame systems are subjected to combined actions sourced from gravity and lateral loads. However, limited information is available on the complex interaction behaviour of such elements affected by different buckling modes. This study aims to provide a better understanding of the behaviour and design of CFS sections under various combinations of compression and bending about both major- and minor-axes. Experimentally validated finite element (FE) models of CFS elements were developed in ABAQUS software, accounting for material nonlinearity and geometric imperfections. The validated models were then used to conduct a parametric study to assess the structural performance and failure modes of over 500 CFS elements with various lengths, thicknesses and cross-sectional dimensions under 19 different load eccentricities. It was demonstrated that the element and web slenderness ratios and the magnitude and direction of eccentricity are the key factors affecting the behaviour of the CFS beam–column elements. The accuracy of current design specifications, including American Iron and Steel Institute (AISI-S100), Australian/New Zealand Standard (AS/NZS-4600) and European standard (Eurocode-3) was then investigated. Subsequently, the results were used to propose a new design interaction equation as a function of element and web slenderness ratios. It was shown that the proposed equation could considerably improve the accuracy of the code strength predictions, especially in the case of medium to high slenderness elements. Finally, a reliability analysis was conducted within the framework of the AISI-S100 to ensure that the proposed design equation provides the required level of safety.

1. Introduction

Cold-formed steel (CFS) elements are increasingly used as primary load-bearing components in low to mid-rise buildings in modular construction [1]. Compared to hot-rolled counterparts, CFS members offer both structural and environmental advantages, such as light weight, flexibility in cross-sectional shapes, ease and speed of construction, greater adaptability in the manufacturing process, recyclability and sustainability [2,3].

In typical multi-storey buildings, many of the primary load-bearing CFS elements act as beam–column elements since they are exposed to combined axial compression and bending actions [4]. In stud-wall systems, the combined loading generally results from applied eccentric compression load (see Fig. 1(a)), mainly attributed to the end connection detail and/or the shift of the effective centroid of the cross-section due to cross-sectional instabilities (e.g., wall studs in ledger framing systems) [5,6]. CFS elements can be also subjected to the transverse loads (see Fig. 1(b)) in combination with the axial compression loads, for example in the stud walls surrounding a building's perimeter [4]. On the other hand, the column elements used in CFS moment-resisting frames are typically under simultaneous axial compression and bending actions (see Fig. 1(c)) [7,8].

Several studies have experimentally and numerically investigated the structural performance of the CFS beam–column members under different load combinations. Torabian et al. [9,10] studied the buckling behaviour and failure mechanism of 55 lipped channel and 43 Z-shaped warping-restrained CFS beam–column members subjected to axial compression and bi-axial bending. The results of these experimental tests confirmed that the simple linear interaction approach suggested by the AISI S100 (2012) [11] provides conservative predictions for the strength of beam–column members. A similar conclusion was made

* Corresponding author.
E-mail address: smmojtabaei1@sheffield.ac.uk (S.M. Mojtabaei).

https://doi.org/10.1016/j.tws.2023.110588
Received 14 August 2022; Received in revised form 27 January 2023; Accepted 28 January 2023
Available online 4 March 2023

Notation

b_f	Flange width of a section
CDF	Cumulative distribution function
CFS	Cold formed steel
C_p	Number of samples
$C_\varnothing$	calibration factor
d_1	Overall depth of lip
DSM	Direct strength method
E	Young's modulus of elasticity
e_y	Eccentricity in y-direction
FE	Finite element
F_m	Fabrication factor
F_y	Yield stress of the material
F_u	Ultimate stress of the material
h	Depth of section
K	Effective length factor
L	Length of a member
L_e	Length of a member
M_{bx}, M_{by}	Nominal member moment capacities about the x-and y-axes, respectively
M_m	Mean values of the material factor
M_{nx}, M_{ny}	Nominal member moment capacities about the x-and y-axes, respectively
M_x, M_y	Applied bending moments about the x-and y-axes, respectively
M_x^*, M_y^*	Applied bending moments about the x-and y-axes, respectively
N_c	Nominal capacity of a member in compression
N^*	Applied axial compression
P	Applied axial compression
P_m	Mean value of the professional factor
P_n	Nominal capacity of a member in compression
P_{Code}	Capacity of beam–columns predicted by the codes' interaction equation
P_{FE}	Predicted capacity of beam–columns obtained through FE models
P_{Test}	Capacity of beam–columns obtained from the reference experiments
P_{Prop}	Capacity of beam–columns predicted by proposed interaction equation
r	Radius of gyration
R	Radius of round corners
r_y	Radius of gyration about the minor-axis
t	Thickness of a channel
V_F	Coefficient of variation of the material factor
V_m	Coefficient of variation of the material factor
V_p	Coefficient of variation of P_m
V_Q	Coefficient of variation of the load effect
β_0	Target reliability index
λ_d	Non-dimensional slenderness used to determine P_{nd} and M_{nd}
λ_s	Cross-sectional slenderness
λ_y	Element slenderness ratio about the minor-axis
$\varnothing$	Resistance factor
ε_e	Measured engineering strain
ε_{true}	True strain
σ_{cr}	Elastic critical local/distortional buckling stress
σ_e	Measured engineering stress
σ_{true}	True stress
$\sigma_{0.2\%}$	Proof stress of the material
ϑ	Poisson's ratio
ω_d	Imperfection magnitude
$\sum \gamma_i Q_i$	Required strength based on the critical load combination
$\varnothing$	Resistance factor

by Li et al. [12] who conducted experimental and numerical investigations on the in-plane behaviour of 57 eccentrically compressed beam–columns.

Hancock and Rasmussen [13] investigated the interaction behaviour of thin-walled beam–columns by using slender cross-section square hollow sections (SHS) and thin-walled I-sections subjected to the combined action of compression and bending about both minor and major principal axes. They concluded that welded I-sections bent along the minor principal axis had convex interaction curves for shorter lengths and concave interaction curves for longer lengths. However, the cross-sections bent along the major principal axis exhibited slightly convex curves over a longer length and failed due to flexural–torsional buckling. In another relevant study, Cheng et al. [14] presented an analytical study on the flexural and lateral–torsional buckling of CFS lipped channel sections subjected to combined axial compression and bending about their major- and minor-axes. It was shown that the bending moment decreases the critical compressive load when CFS sections were subjected to combined compression and major-axis bending. On the other hand, for a section subjected to combined compression and minor-axis bending, the influence of the bending moment on the critical compression load was found to be dependent on the direction of the applied moment. When the minor-axis bending moment compressed the lips, the critical value of the compressive load was reduced; however, the direction of the bending moment compressing the web had almost no effect on the critical value of the compression load unless the applied moment was close to the design flexural capacity of the member.

Ma et al. [15] conducted an experimental investigation on 51 short high-strength CFS elements with square and rectangular hollow sections subjected to combined compression and bending by adopting different eccentricities. The results showed that the interaction equations proposed by American [16], European [17], and Australian design provisions [18] can provide, on average, 13%–21% conservative predictions. In another study, Li and Young [19] assessed the interaction equations for the CFS built-up open sections under different eccentric loads through experimental investigations. It was concluded that the current CFS design standards (i.e., AISI S100 [20], AS/NZS 4600 [21], EN 1993-1-1 [17] and ANSI/AISC 360 [22]) generally underestimate the strength of the CFS built-up open section beam–columns. In a follow-up study [23], they improved the interaction equation for the design of beam–columns with built-up sections.

A number of research studies aimed to optimise the cross-sectional shapes and dimensions of single and built-up beam–columns in order to maximise their load-bearing capacities under various load combinations [4,24,25]. Wang et al. [24] and Parastesh et al. [25] determined optimum cross-sectional shapes for singly-symmetric and anti-symmetric CFS beam–column members subjected to different combinations of axial compressive loads and bending moments about the major-axis, respectively. In another study, Mojtabaei et al. [4] demonstrated that by changing the relative cross-sectional dimensions, the

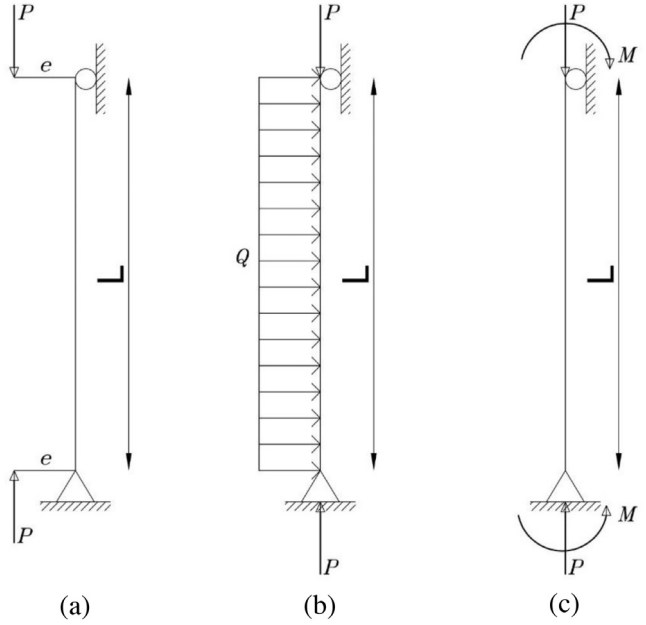

Fig. 1. Beam–column member subjected to (a) eccentric axial load; (b) combined axial compression and transverse load; and (c) combined axial compression and bending.

strength of CFS beam–column members with various single and built-up cross-sections can be improved by up to 156%.

In a more recent study, Hasanali et al. [26] evaluated the accuracy of available methods for the estimations of the load-carrying capacity of the CFS warping-restrained beam–column members. Following a comprehensive parametric study using experimentally validated Finite Element (FE) models, it was demonstrated that in comparison to other methods, the Direct Strength Method (DSM) generated the most conservative predictions for beam–column members by up to 55%. This can be attributed to errors associated with (i) warping-restrained boundary condition effects, (ii) equations for the calculations of buckling loads, and (iii) the AISI linear interaction equation used in this method. In another relevant study, Öztürk et al. [27] investigated the structural behaviour of eccentrically loaded beam–column CFS lipped and sigma channel profiles through an experimental and analytical study. It was demonstrated that using sigma sections for the short beam–columns generally results in higher strength by up to 42% compared to those with lipped channel sections. In addition, they found that AISI [20] and Eurocode 3 (EC3) [28] generally underestimate the capacity of CFS beam–column members, on average, by around 50% and 25%, respectively.

Despite this rather large body of research on the behaviour of CFS specimens subjected to combined loading, little attention has been paid to assessing the behaviour of the CFS single sections under various combinations of axial compressive loads and bending moments. The accuracy of the current design standards, including AISI S100 [20], AS/NZS 4600 [21] and EC3 [28–30], in the strength predictions of CFS beam–columns was first evaluated in this study. An empirical nonlinear interaction equation was then proposed to provide more reliable design solutions for the design of CFS beam–column elements with single channel sections. To this end, detailed nonlinear FE models of CFS beam–column members under various load combinations were developed by taking into account material nonlinearity and geometric imperfections and then validated against the results of experimental tests. The validated models were then utilised for a comprehensive parametric study that contains 513 FE models, covering a wide range of key design parameters, such as length (i.e., 0.5, 1.5, 3 *m*), thickness (i.e., 1, 2, 4 *mm*) and cross-sectional dimensions under 19 different load eccentricities. Finally, the results were employed to develop a more accurate interaction equation for the design of CFS beam–column members, while its adequacy for practical applications was demonstrated by conducting a reliability analysis.

2. Code-prescribed buckling resistance of beam–column elements

To predict the load-carrying capacity of CFS beam–column elements, the first step is to determine their strength under pure axial compression and pure bending actions. This can be achieved by adopting the traditional effective width method (EWM) prescribed by the European design guideline [28]. The Direct Strength Method (DSM) [31], which is available in AISI S100 [20] and AS/NZS 4600 [21], can be also used as an alternative method to estimate the nominal pure compressive and bending strength values. While yield strength and reduced cross-section properties are used in the EWM, the DSM is a function of gross cross-section properties, and a reduced strength value is calculated based on the stability of the gross cross-section. The current design regulations for CFS beam–column members are briefly summarised in the following sections.

2.1. North American and Australian/New Zealand design standards

To determine the strength of a member subjected to multiple actions, the typical approach in steel design is to employ an interaction equation. For a CFS member under combined compression and bending actions, a simplified linear interactive equation recommended by AISI S100 [20] (Eq. (1)) and AS/NZS 4600 [21] (Eq. (2)) is generally employed:

$$\frac{P}{P_n}+\frac{M_x}{M_{nx}}+\frac{M_y}{M_{ny}}\le 1.0 \tag{1}$$

$$\frac{N^*}{N_c}+\frac{M_x^*}{M_{bx}}+\frac{M_y^*}{M_{by}}\le 1.0 \tag{2}$$

In the above equations, P, M_x and M_y (N^*, M_x^* and M_y^* in AS/NZS 4600 [21]) are defined as the applied axial compression load and bending moments about the x- and y-axes, respectively. P_n (N_c in AS/NZS 4600 [21]) denotes the nominal axial compressive capacity, while M_{nx} and M_{ny} (M_{bx} and M_{by} in AS/NZS 4600 [21]) are nominal flexural strength about the x- and y-axes, respectively. Nominal pure strength (P_n, M_{nx} and M_{ny}) is typically determined by the DSM equations supplied in Chapters E and F of the AISI S100 [20] as well as Chapter 7 of AS/NZS 4600 [21].

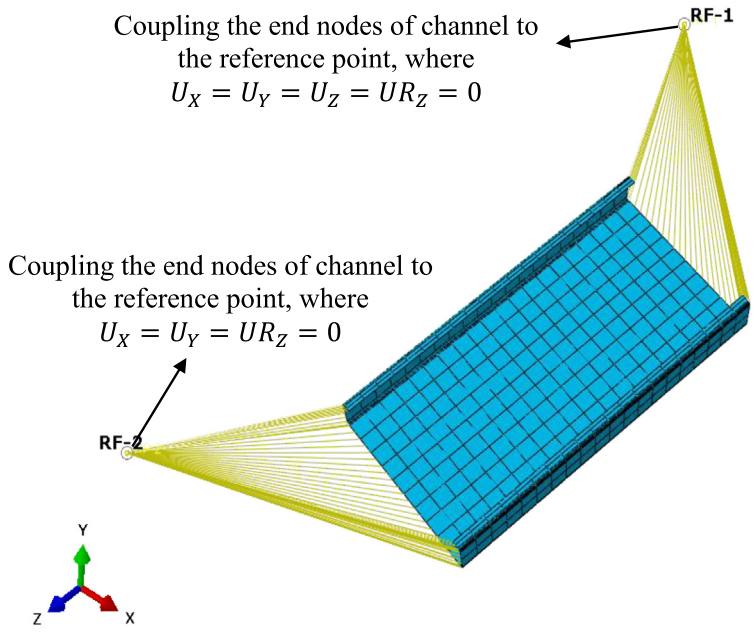

Fig. 2. CFS element boundary conditions under eccentric compressive loads.

2.2. European design standard

According to EC3 [28–30], the strength of CFS beam–columns is taken as the minimum of the following two resistances: (i) cross-sectional resistance and (ii) member buckling resistance.

As outlined in Clause 8.1.8 of EC3 Part 1–3 [28], the cross-section of a CFS beam–column subjected to the combined action of axial compression (N_{Ed}) and bending moments ($M_{y,Ed}$ and $M_{z,Ed}$) should satisfy the following criteria:

$$\frac{N_{Ed}}{N_{c,Rd}} + \frac{M_{x,Ed} + \Delta M_{x,Ed}}{M_{cx,Rd,com}} + \frac{M_{y,Ed} + \Delta M_{y,Ed}}{M_{cy,Rd,com}} \leq 1.0 \tag{3}$$

where $N_{c,Rd}$ denotes the design resistance of the cross-section in uniform compression. $M_{cx,Rd,com}$ and $M_{cy,Rd,com}$ are the design bending moment resistance of the cross-section about the major (x) and minor (y) axes, respectively, using the section modulus for the compression side. The factors $\Delta M_{x,Ed}$ and $\Delta M_{y,Ed}$ are defined as the additional bending moments generated by the shift of the centroidal axes of the effective cross-section relative to those of the gross cross-section, which are estimated by:

$$\Delta M_{x,Ed} = N_{Ed} e_{Ny} \tag{4}$$

$$\Delta M_{y,Ed} = N_{Ed} e_{Nx} \tag{5}$$

where e_{Nx} and e_{Ny} are the shift of the x- and y-axes, respectively.

With respect to the member resistance, the following interaction equations are recommended by Clause 8.2.5 of EC3 Part 1–3 [28] for two different buckling axes:

(i) Major principal axis buckling:

$$\left(\omega_{z,x} \frac{N_{Ed}}{\chi_x N_{c,Rd}}\right)^{\alpha_x} + \left(\omega_{z,LT} \frac{M_{x,Ed} + \Delta M_{x,Ed}}{\chi_{LT} M_{cx,Rd}}\right)^{\beta_x} + \left(\frac{M_{y,Ed} + \Delta M_{y,Ed}}{M_{cy,Rd}}\right)^{\delta_x} \leq 1.0 \tag{6}$$

(ii) Minor principal axis buckling:

$$\left(\omega_{z,y} \frac{N_{Ed}}{\chi_y N_{c,Rd}}\right)^{\alpha_y} + \left(\omega_{z,LT} \frac{M_{x,Ed} + \Delta M_{x,Ed}}{\chi_{LT} M_{cx,Rd}}\right)^{\beta_y} + \left(\frac{M_{y,Ed} + \Delta M_{y,Ed}}{M_{cy,Rd}}\right)^{\delta_y} \leq 1.0 \tag{7}$$

In the above equations, $M_{cx,Rd}$ and $M_{cy,Rd}$ are defined as the bending moment resistances of the cross-section about the x- and y-axes, respectively, which are calculated using the EWM regulations [30]. χ_x and χ_y are the reduction factors for flexural buckling about the x- and y-axes, respectively, and χ_{LT} denotes the reduction factor for lateral–torsional buckling, given by EC3 Part 1-1 [29]. In the case of torsional-flexural buckling, the relevant reduction factor for flexural buckling, χ_x or χ_y, should be replaced with χ_{TF} [28]. $\omega_{z,x}$ and $\omega_{z,y}$ denote the interpolation factors, which depend on the location of the cross-section under evaluation and account for the relevant buckling mode. The exponents of Eqs. (6) and (7) (α_x, α_y, β_x, β_y, δ_x and δ_y) are defined according to the following formulas:

$$\begin{aligned} &\alpha_x, \beta_x, \delta_x = \chi_x/\omega_{z,x} \geq 0.85 \\ &\alpha_y, \beta_y, \delta_y = \chi_y/\omega_{z,y} \geq 0.85 \end{aligned} \tag{8}$$

3. Description of Finite Element (FE) models

It has been previously demonstrated that FE simulations using ABAQUS software [33] can be used as an efficient and reliable tool to predict the structural performance of thin-walled CFS elements and connections under various loading conditions [34,35]. In this study, the results of an experimental programme conducted by Torabian et al. [32] at Johns Hopkins University on CFS elements under combined axial compression and bending moments (i.e., beam–columns) were used to validate detailed nonlinear FE models accounting for the material nonlinearity and geometric imperfections. The following is a summary of the models' main features.

3.1. Specimens, boundary conditions and loading

The boundary conditions of the experimental test set-up were replicated in the FE models, as demonstrated in Fig. 2. Two reference points were placed at the end sections of the lipped channel elements to simulate the support and applied eccentric compression. As shown in Fig. 2, the nodal degrees of freedoms at each end of the element were then coupled to their respective reference point which was pinned about the minor- and major-axes. The coordinates of the reference points were varied to apply different eccentricities to the element. While a concentrated load was applied to one of the reference points in a force-control manner (Rf-2 in Fig. 2), the other reference point was restrained in the longitudinal direction (U_z) to simulate the support.

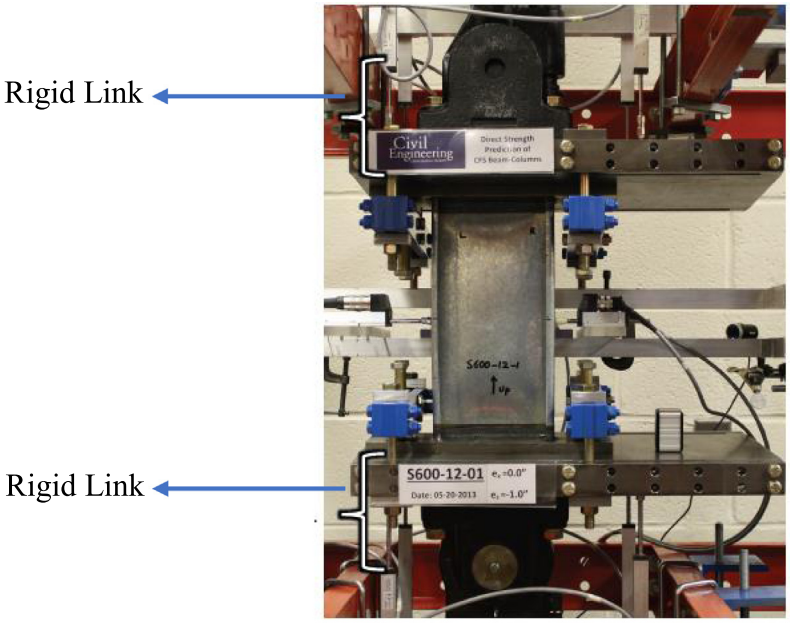

Fig. 3. Lipped channel cross-section tested by Torabian et al. [32].

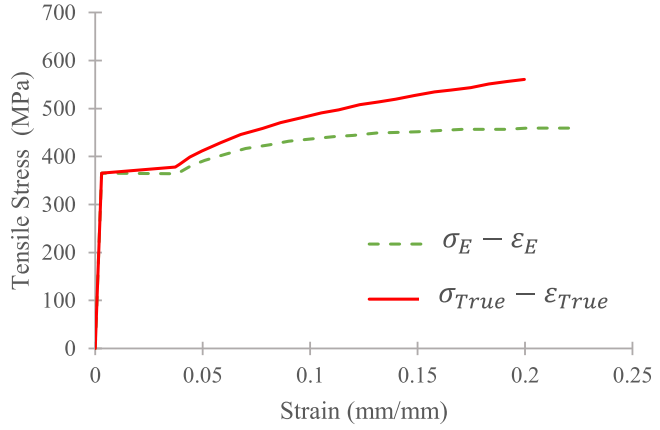

Fig. 4. Material stress–strain relationship used in FE models (adopted from Torabian et al. [32]).

Finally, a rigid link with a length of 152.4 *mm* in the longitudinal direction was created between the reference points and the ends of the specimen to account for the depth of the clevis employed in the test set-up (see Fig. 3)

3.2. Element type and material properties

Shell elements are the logical choice to simulate the behaviour of thin-walled elements, where their thickness is considerably smaller than the other dimensions [7]. In the present study, a nine-node shell element using quadratic shape functions, $S9R5$, was assigned to the elements in ABAQUS software [33]. Each node of this element type has five degrees of freedom, with three displacements and two in-surface rotational components. While $S9R5$ is a robust element type allowing as little as one element per buckling half-wave without degrading the solution, it can provide accurate predictions for thin-walled structures according to Schafer et al. [36].

A detailed mesh sensitivity analysis was conducted to investigate the impact of mesh density on the results. The estimated compressive strength along with the analysis time for one of the CFS members (i.e., the S600-305-11 cross-section adopted from Torabian et al. [32]) with various mesh sizes are reported in Table 1. It can be concluded that the refinement of the mesh size beyond 10 × 10 mm^2 had a negligible effect on the predicted compression capacity of the cross-section whilst considerably increasing the computational time. Consequently, in this study element sizes of 10 × 10 mm^2 were adopted for the flat regions of the CFS elements, whereas four elements were used in the radial direction of their corners.

Table 1
Mesh sensitivity analysis of cross-section S600-305-11.

Element size mm^2	Time (s)	Predicted capacity (kN)
5 × 5	701	20.897
10 × 10	135	20.870
15 × 15	66	20.879
25 × 25	28	20.910

A true stress–strain model was used to simulate the behaviour of CFS elements. The engineering stress–strain curves obtained from coupon tests [32] were converted to true stress and true strain data using the following equation:

$$\begin{cases} \varepsilon_{true} = \ln(1+\varepsilon_e) \\ \sigma_{true} = \sigma_e(1+\varepsilon_e) \end{cases} \quad (9)$$

where σ_e and ε_e are the measured engineering stress and strain values based on the original cross-sectional area of the coupons, respectively. The engineering and true stress–strain curves of the tested beam–column elements are shown in Fig. 4. The measured Poisson ratio, Young's modulus of elasticity, the yield stress, and the ultimate stress of the CFS material are equal to $\upsilon = 0.3$, $E = 203.4$ *GPa*, $F_y = 365$ *MPa*, and $F_u = 560$ *MPa*, respectively.

3.3. Geometric imperfections

The stability of thin-walled CFS members may be significantly affected by the presence of initial geometric imperfections due to their influences on the strength and post-buckling behaviour of the elements [37,38]. Based on the work carried out by Schafer and Peköz [31], the dominant buckling mode shape derived from elastic buckling analysis can be employed to determine the general shape of imperfections. In this study, the Finite Strip Method was first used to

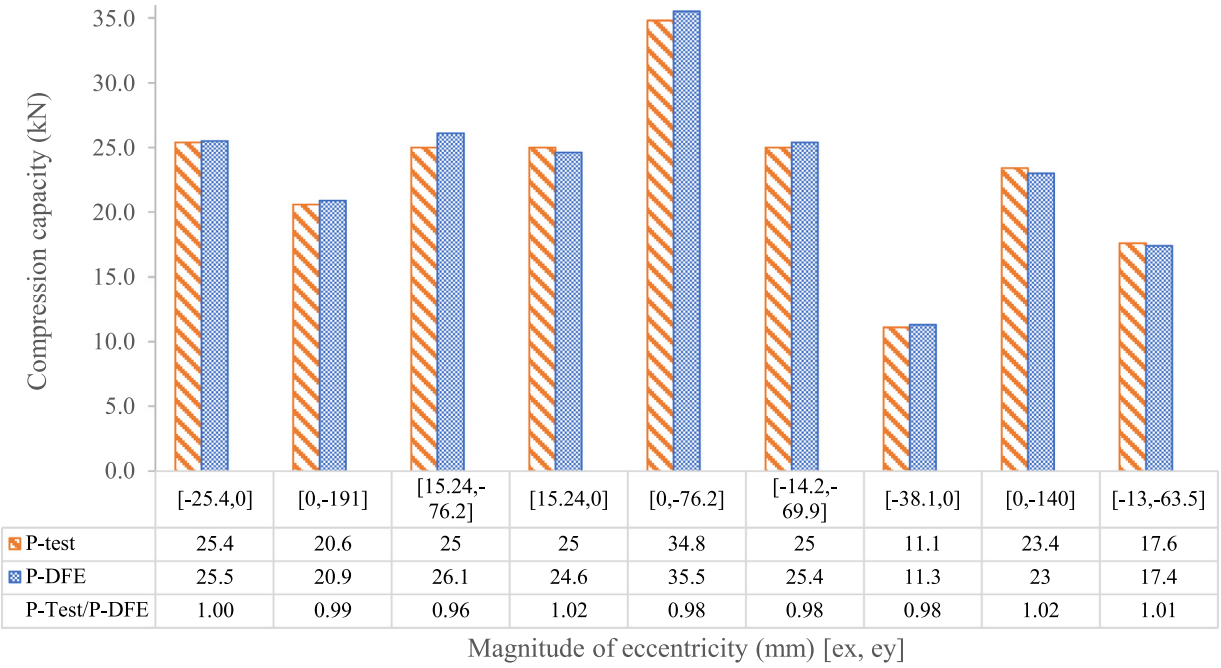

	[-25.4,0]	[0,-191]	[15.24,-76.2]	[15.24,0]	[0,-76.2]	[-14.2,-69.9]	[-38.1,0]	[0,-140]	[-13,-63.5]
P-test	25.4	20.6	25	25	34.8	25	11.1	23.4	17.6
P-DFE	25.5	20.9	26.1	24.6	35.5	25.4	11.3	23	17.4
P-Test/P-DFE	1.00	0.99	0.96	1.02	0.98	0.98	0.98	1.02	1.01

Fig. 5. Comparison of CFS beam–column capacities derived from reference experimental tests (P_{Test}) and FE models (P_{DFE}).

predict the dominant buckling mode shape and its corresponding half-wavelength for each element [39]. For the CFS element with a thickness (t) smaller than 3 *mm*, the magnitude of the buckled shape was scaled to $0.34t$ and $0.94t$ for local buckling and distortional buckling, respectively, which corresponds to a Cumulative Distribution Function (CDF) value of 50% according to Schafer and Peköz [40]. For the specimens with a thickness (t) exceeding 3 *mm*, the imperfection magnitude was determined using the equation proposed by Walker [41]:

$$\omega_d = 0.3t\sqrt{\frac{\sigma_{0.2\%}}{\sigma_{cr}}} = 0.3t\lambda_s \tag{10}$$

where $\sigma_{0.2\%}$ and σ_{cr} are 0.2% proof stress of the material and elastic critical local/distortional buckling stress of the cross-section, and λ_s is the cross-sectional slenderness, given by:

$$\lambda_s = \sqrt{f_y/\sigma_{cr}} \tag{11}$$

A value of $L_e/1500$ (where L_e is the length of the member), as reported in previous studies [42,43], was also taken for the overall buckling imperfection magnitude. It should be noted that either a local or a distortional imperfection was incorporated into the FE models of short elements, depending on which mode had the lower critical buckling stress [42], while a combination of three buckling modes (i.e. local, distortional, and global) was introduced for the medium and long-length members [32].

3.4. Validation of the FE models

The accuracy of the developed FE models of the beam–columns was validated against the experimental results of the study by Torabian et al. [32]. To predict the capacity of the CFS elements, a nonlinear inelastic post-buckling analysis was performed in ABAQUS [33] using the standard RIKS arc-length method. Table 2 demonstrates the cross-sectional dimensions and lengths of the beam–column specimens subjected to compressive loads with nine different eccentricity values on the major- (x) and minor-(y) axes. The selected eccentricities imposed different combined actions on the CFS element, including: (i) compression and a negative minor-axis bending moment, (ii) compression and a positive minor-axis bending moment, (iii) compression and a major-axis bending moment, and (iv) compression and bi-axial bending moments.

The compressive capacities of the CFS beam–column members predicted by the FE models (P_{DFE}) and experiments (P_{Test}) are compared in Fig. 5, showing a maximum estimation error of 4% and a standard deviation of 0.02. Fig. 6 compares the axial force–displacement curves of test specimens, namely S600-610-8 and S600-1219-9, and those obtained from FE simulations. It can be seen that the developed FE models could accurately predict the behaviour of CFS beam–columns over the entire loading range, including peak load, initial stiffness, ultimate capacity, and post-buckling behaviour. It should be noted that the slight difference between the initial stiffness of the tested specimens and the FE models can be attributed to the minor detachment of the end plate and loading plates as well as a small movement in the test rig's swivel joints [35]. The failure modes predicted by the FE were also in good agreement with those observed during experimental tests, as shown in Fig. 7 for the S600-610-8 specimen under combined compression and bending about the major-axis.

4. Parametric study

A comprehensive parametric study was conducted, using the experimentally validated FE models described in the previous section, to investigate the efficiency of the code-prescribed compressive load-bending moment interaction equations and develop a more accurate interaction formulation for the CFS beam–columns.

As shown in Table 3 and Fig. 8, three sets of cross-sectional dimensions ($C1$, $C2$ and $C3$) with the thicknesses of 1 *mm*, 2 *mm* and 4 *mm* and the lengths of 500 *mm* (short), 1500 *mm* (medium) and 3000 *mm* (long) were selected to determine the effects of key design parameters. The selected cross-sections cover a wide range of both overall ($\lambda = KL/r$) and web (h/t) slenderness ratios, where K, L, and r are defined as effective length factor, unbraced length of member and radius of gyration, respectively, and h and t denote the flat depth and the thickness of the web, respectively.

The effects of all possible combinations of axial compressive load and bending moments, including combined compression and major-axis bending, combined compression and minor-axis bending and combined compression and bi-axial bending, were evaluated by selecting 15 different combinations of loading conditions. Furthermore, the capacities of the cross-sections in the anchor points of the interaction curves

Table 2
Experimental tests' variables [32].

Section name	Web height	Flange	Lip	Thickness	Radius of round corners	Length	Eccentricities	
	h (mm)	b_f (mm)	d_1(mm)	t (mm)	R (mm)	L (mm)	e_x (mm)	e_y (mm)
S600-305-1							−25.4	0
S600-305-11						305	0	−191
S600-305-15							15.24	−76.2
S600-610-5							15.24	0
S600-610-8	152.05	34.95	9.52	1.45	2.87	610	0	−76.2
S600-610-15							−14.2	−69.9
S600-1219-1							−38.1	0
S600-1219-9						1219	0	−140
S600-1219-15							−13	−63.5

Negative eccentricity in the x direction shows that the web of the specimens is in compression.

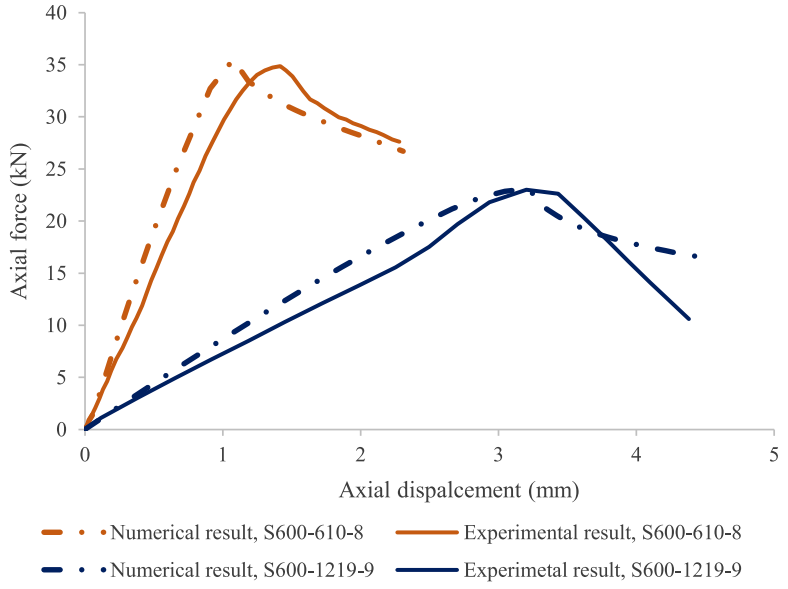

Fig. 6. Axial force–displacement relationship resulting from reference experimental tests against FE models for S600-610-8 and S600-1219-9 beam–columns.

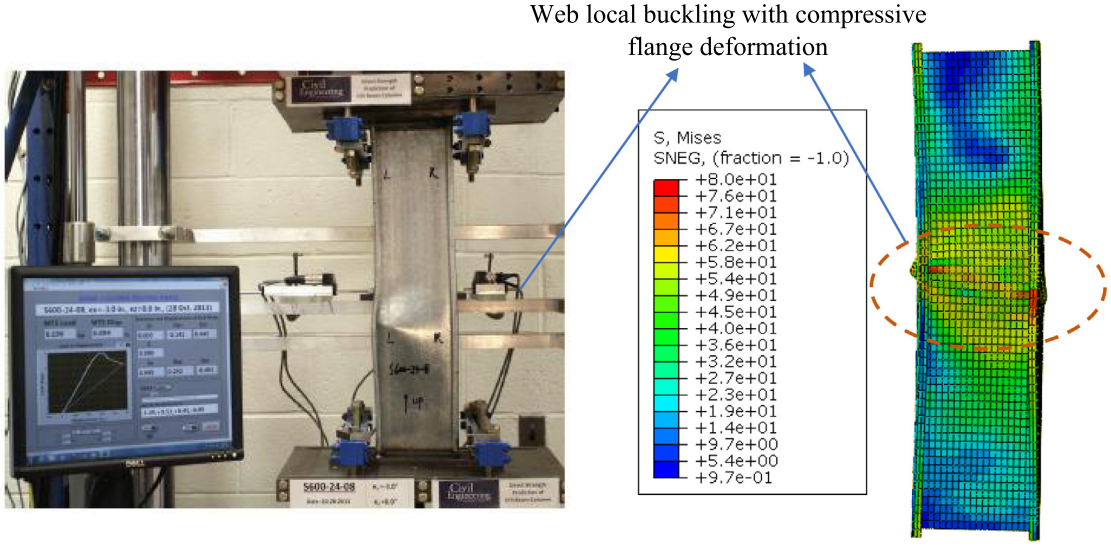

Fig. 7. Failure mode determined by FE model versus experimental (S600-610-8) (test set-up adopted from Torabian et al. [32]).

were predicted using four alternative loading conditions, consisting of pure compression, pure bending about the major-axis, and pure minor-axis bending in two directions (i.e., bending moments putting the web in compression or tension). These possible loading combinations were applied using various eccentricity values, as listed in Table 4. To account for the effects of the aforementioned design variables on the capacity of the beam–columns, a total of 513 FE models were developed. The yield stress (F_y), the ultimate stress (F_u), the elastic

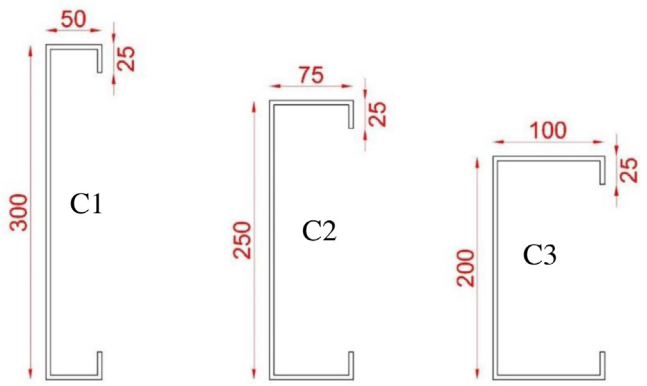

Fig. 8. Cross-sectional geometry of the specimens.

Table 3
Parametric study variables.

Section name	Thickness	Length
	t (mm)	L (mm)
$C1$ $C2$ $C3$	1, 2 and 4	500, 1500 and 3000

Table 4
Magnitude of the eccentricities.

Loading condition	Eccentricities	
	e_x (mm)	e_y (mm)
Pure compression	0	0
Pure bending about major-axis	0	∞
Pure bending about minor-axis (web in compression)	-∞	0
Pure bending about minor-axis (web in tension)	∞	0
Minor-axis bending + compression load	10	0
	−10	0
	25	0
	−25	0
	50	0
	−50	0
Major-axis bending + compression load	0	10
	0	100
	0	200
Bi-axial bending moment + compression load	10	10
	−10	10
	25	100
	−25	100
	50	200
	−50	200

Negative eccentricity in the x direction shows that the web of the specimens is in compression.

modulus (E), and the Poisson's ratio of the material (ϑ) were taken as 440 *MPa*, 600 *MPa*, 207 *GPa*, and 0.3, respectively.

5. Results and discussions

Table 4 shows the direction and magnitude of the selected eccentricities used in this study. Three negative and three positive eccentricities (e_x) which put the web in compression and tension, respectively, were employed to assess the combinations of a compressive load and a minor-axis bending. Three different eccentricities along the y-axis (e_y) were also selected to generate the combinations of a compressive load and a major-axis bending. Finally, combinations of a compressive load and a bi-axial bending were imposed on the CFS elements using six eccentricity-couples (e_x, e_y). The behaviour of the CFS elements was first assessed by using normalised two-dimensional (2D) strength interaction surfaces ($P - M$) under combinations of compression load and bending moments about either a major- or minor-axis. The capacities of the beam–columns were then examined in three-dimensional (3D) space ($P - M_x - M_y$) to determine the accuracy of the interaction equation (Eq. (1)) prescribed in AISI S100 [20] and AS/NZS 4600 [21] under all selected eccentricities. The capacities of the beam–column members predicted by the validated FE models were then compared to those estimated using the EC3 guidelines [28]. Following that, by using an optimisation process, the errors between the results of the detailed FE models and the strength values estimated from the proposed equation (P_{Prop}) were minimised to develop a more accurate interaction equation for the design of CFS beam–columns. Lastly, the accuracy of the proposed equation was evaluated for two distinct standard CFS lipped channel sections being used in New Zealand (NZ) with different cross-section sizes compared to those used to develop the proposed equation.

5.1. Assessment of beam–columns under major-axis bending

Figs. 9–11 illustrate the normalised peak compressive loads (P/P_n) and major-axis bending moments (M_x/M_{nx}) obtained from the validated FE models in the 2D interaction space. It should be noted that the anchor points of Figs. 9–11 are P_n and M_{nx} obtained from the FE analyses on the CFS elements under pure compression and pure major-axis bending, respectively (see Section 2). The main difference between these figures is in terms of the element slenderness ratio about the minor-axis ($\lambda_y = KL/r_y$), where r_y is the radius of gyration about the minor-axis. For better comparison, the data points are divided into three categories: (i) low slenderness ratios $\lambda_y \leq 50$ (see Fig. 9), (ii) medium slenderness ratios $50 < \lambda_y \leq 100$ (see Fig. 10) and (iii) high slenderness ratios $\lambda_y > 100$ (see Fig. 11). As expected, in all cases the presence of a major-axis bending moment led to a reduction in the maximum compressive capacity of the CFS element. However, the reduction rate seems to be affected by the slenderness ratio of the elements.

It can be seen from Fig. 9 that the code-prescribed interaction curve (Eq. (1)) may lead to either underestimated or overestimated strength predictions for the CFS elements with low slenderness ratios (i.e., $\lambda_y \leq 50$), while on average provides reasonable predictions. In general, it is evident that the interaction equation could predict the strength of the beam–columns under low eccentricities (i.e., circle (1) in Fig. 9) with a higher level of accuracy compared to those under larger eccentricities.

Fig. 12 illustrates failure modes of the CFS elements with slenderness ratios of 18.1 and 39.9 under various eccentricities extracted from the FE models. The web local buckling was observed in the elements under low eccentricities (i.e., $e_y = 10$ *mm*), which act similar to pure compressive members. By increasing the eccentricity of the applied compressive load, the CFS elements failed in either a distortional mode or an interactive local-distortional mode which was initiated from the web local buckling and then involved the distortional buckling of the compressive flange.

Fig. 10 indicates that the interaction equation (Eq. (1)) provided conservative estimations of the strength of CFS beam–columns with medium slenderness ratios (i.e., $50 < \lambda_y \leq 100$) as the data points generally fell above Eq. (1). The typical failure modes of these elements were shown in Fig. 13 Similar to the low-slender specimens, the web local buckling was observed in the CFS elements with medium slenderness ratios subjected to low eccentricities (i.e., $e_y = 10$ *mm*). The position of these elements within the normalised $P - M_x$ space was specified by circle (1) in Fig. 10. For the majority of other specimens, either distortional or combined local-distortional buckling were observed

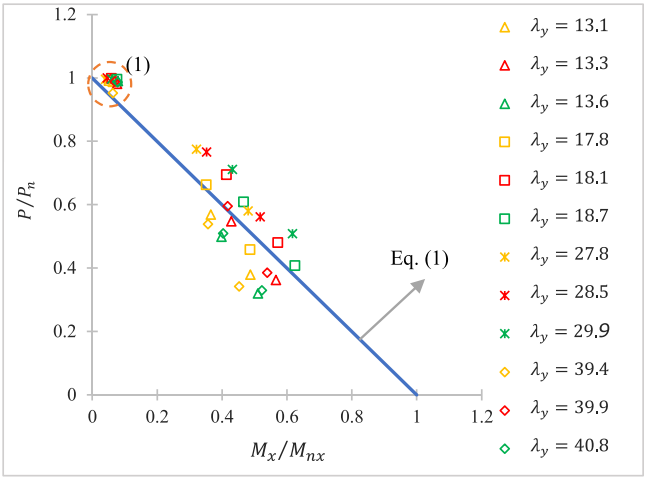

Fig. 9. Interaction of P/P_n and M_x/M_{nx} for CFS beam–columns with low slenderness ratio ($\lambda_y \leq 50$).

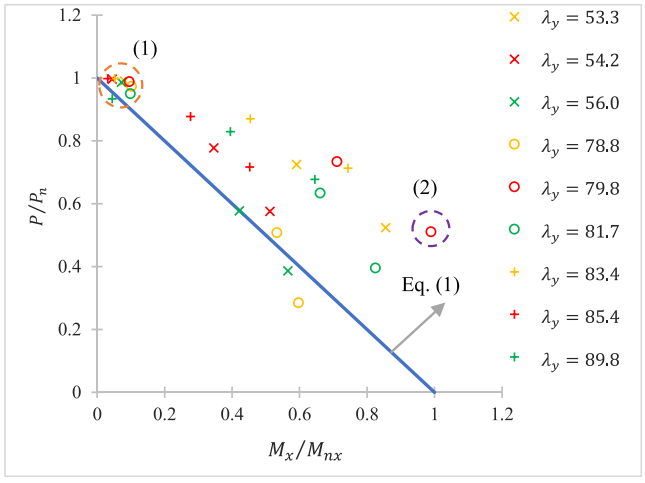

Fig. 10. Interaction of P/P_n and M_x/M_{nx} for CFS beam–columns with medium slenderness ratio ($50 < \lambda_y \leq 100$).

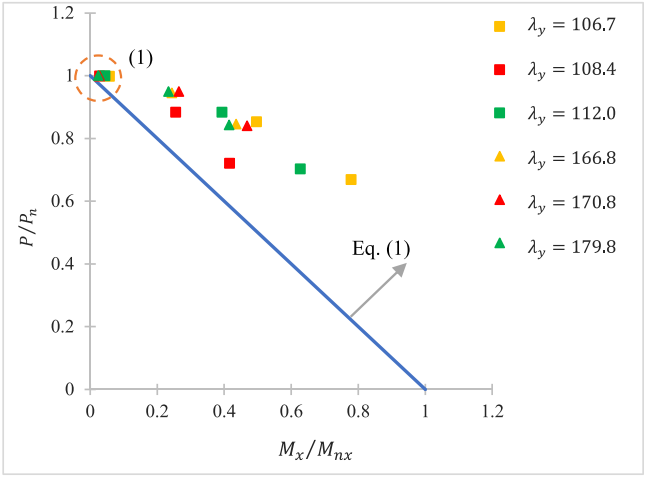

Fig. 11. Interaction of P/P_n and M_x/M_{nx} for CFS beam–columns with high slenderness ratio ($\lambda_y > 100$).

depending on the cross-sectional thickness and the eccentricity level. While the specimens with the low thickness (i.e., $t = 1$ *mm*) experienced severe local buckling in their webs, increasing the eccentricity generated distortional deformations in the compressive flanges of the elements (see Fig. 13(a)). For the elements with thicker plates (i.e., $t = 4$ *mm*), the contribution of the web local buckling was diminished by increasing the eccentricity, and consequently the dominant failure mode changed to flange distortional buckling, as shown in Fig. 13(b). It should be noted that there was an inconsistent data point in the normalised $P - M_x$ space of Fig. 10 specified by circle (2), where the CFS element failed in global buckling followed by web local buckling and flange distortional buckling (see Fig. 13(c)).

It can be seen from Fig. 11 that the strength of CFS beam–columns with high slenderness ratios (i.e., λ_y >100) was always underestimated by using the code-prescribed interaction equation. The results also demonstrate that, regardless of the applied eccentricities, all high-slender beam–columns experienced web local buckling and/or flange distortional buckling which was followed by global instability. Fig. 14 demonstrates the failure modes of the CFS specimens with slenderness ratios of 108.4 and 179.6 under low (i.e., $e_y = 10$ *mm*) and high eccentricities (i.e., $e_y = 200$ *mm*) obtained from the FE models. In general, by comparing Figs. 9–11, it can be concluded that the presence of global buckling and increasing the eccentricity levels increased the errors obtained from the strength predictions of the code-prescribed interaction equation (Eq. (1)). This highlights the need to develop more accurate design equations for such cases.

5.2. Assessment of beam–columns under minor-axis bending

The behaviour of the CFS beam–columns subjected to the combined compressive load and minor-axis bending moment is investigated in this section. Figs. 15–17 show the normalised peak compressive loads (P/P_n) and minor-axis bendings (M_y/M_{ny}) predicted by the validated FE models in 2D interaction space. Similar to Section 5.1, the anchor points of Figs. 15–17 (i.e., P_n and M_{ny}) were obtained from the FE analyses on the CFS elements under pure compression and pure minor-axis bending. In this case, it was found that categorising the data points based on the cross-sectional web slenderness ratio (h/t) helps in a better understanding of the beam–column behaviour. Thereby, the specimens were divided into three categories: (i) low web slenderness ratio $h/t <$ 100, (ii) medium web slenderness ratio $100 \leq h/t < 200$ and (iii) high web slenderness ratio $h/t \geq 200$.

The results of this study indicate that the parameters that can considerably affect the accuracy of the prescribed interaction equation (Eq. (1)) in AISI S100 [20] and AS/NZS 4600 [21] for the elements under compression and minor-axis bending are: (i) the web slenderness ratio and (ii) the direction of the eccentricity. It can be seen from Fig. 15 that almost all data points belonging to the elements with the low web slenderness (i.e., $h/t < 100$) were positioned below the interaction curve (Eq. (1)). This implies that using the proposed interaction equation in AISI S100 [20] leads to unsafe strength predictions of the low web slenderness elements subjected to compression and minor-axis bending. On the other hand, for the specimens with the medium (i.e., $100 \leq h/t < 200$) and high (i.e., $h/t \geq 200$) web slenderness, Eq. (1) led to either underestimated or overestimated results, mainly when combined compression and positive minor-axis bending or combined compression and negative minor-axis bending was imposed, respectively.

Fig. 18 illustrates the failure modes of the beam–columns with different web-slenderness ratios under various combinations of compression and minor-axis bending. It is shown that the dominant failure mode of the beam–columns under combined actions of compression and negative minor-axis bending (i.e., web in compression) is interactive local-distortional buckling (see Fig. 18(a)). On the contrary, imposing the combined compression and positive minor-axis bending on the elements (i.e., web in tension) induced distortional buckling in the flanges

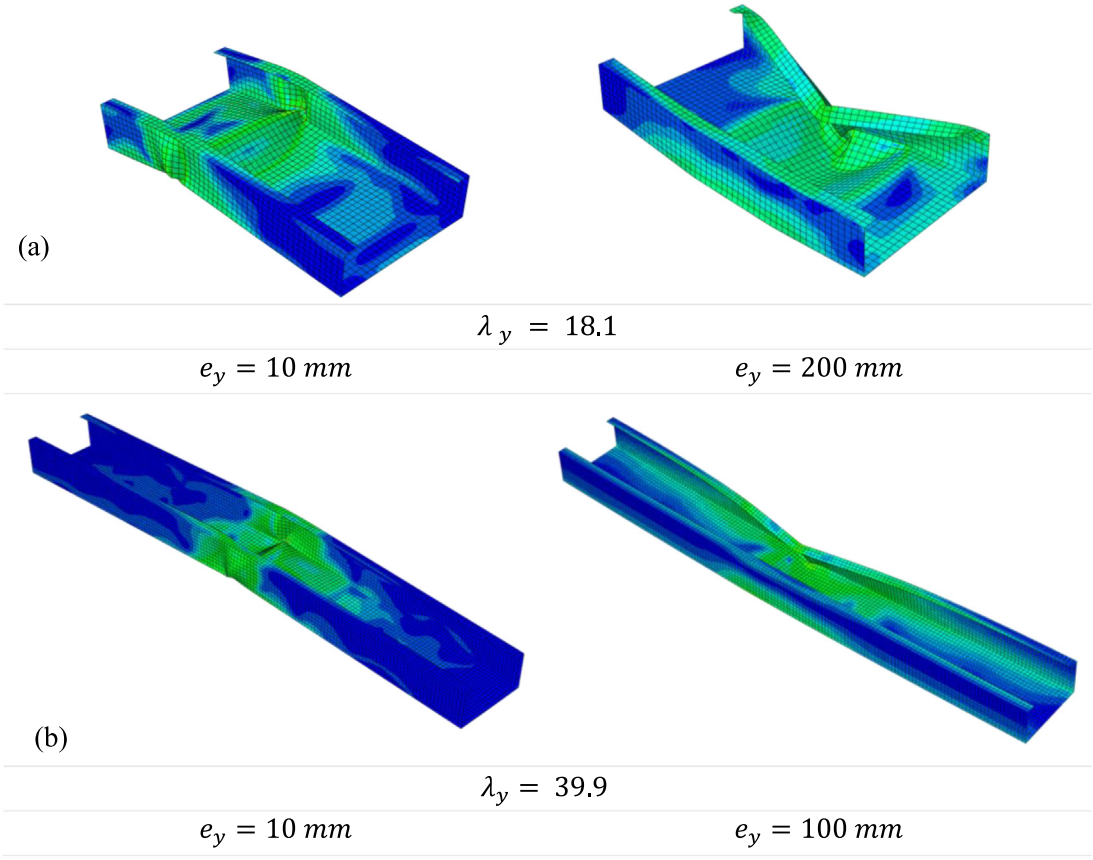

Fig. 12. Failure modes of CFS beam–columns with low slenderness ratio ($\lambda_y \leq 50$) subjected to combined compression and major-axis bending actions.

of the specimens, as shown in Fig. 18(b). For the long length elements (i.e., 3000 *mm*), the aforementioned failure modes were followed by the global buckling (see Fig. 18(c)).

It can be noted that a number of beam–column elements with the medium and high web slenderness ratios under combined compression and positive minor-axis bending exhibited higher strength than those under pure compression. These data points are specified by circle (1) in the normalised $P - M_y$ spaces in Figs. 16 and 17 correspond to the specimens with thin plate thicknesses (i.e., $t = 1$ and 2 *mm*) and the low eccentricity (i.e., $e_x = 10$ *mm*). In these cases, the higher capacity under combined actions can be justified by the effect of the tensile stresses emerged from the bending in the web of the cross-section, which led to a delay in the web's local buckling. However, applying higher eccentricities (i.e., $e_x = 25$ or 50 *mm*) induced significant compressive stresses into the flanges caused by the minor-axis bending and consequently resulted in the distortional buckling of the flanges.

5.3. Assessment of the code-prescribed interaction equations

5.3.1. North American and Australian/New Zealand design standards

To assess the efficiency of the interaction equation suggested by AISI S100 [20] and AS/NZS 4600 [21], the inaccuracy of the DSM equations in estimating the pure nominal strength values was excluded from the interaction equation (Eq. (1)) [26]. To this end, the axial compressive strength (P_n) and flexural capacities (M_{nx} and M_{ny}) of the sections, here called nominal pure capacities, were determined using experimentally validated FE models of the CFS elements with warping-restrained boundary conditions (see Section 3). The predicted P_n, M_{nx} and M_{ny} obtained from FE analyses (see Section 2) are listed in Table 5.

Based on the evaluation carried out on 2D interaction space (Sections 5.1 and 5.2), the accuracy of the interaction equation prescribed in [20,21] can be affected by: (i) λ_y, (ii) h/t and (iii) the value and direction of e_y and e_x. To quantify the accuracy of the code-prescribed interaction equation (Eq. (1)), in this section, the strength of the CFS beam–columns predicted by the detailed FE models are compared to those estimated by Eq. (1) for a wide range of elements. The concentrated bending moments about the major- (M_x) and minor-axes (M_y) were generated on the end sections of the CFS elements by imposing compressive load (P) with eccentricities along y (e_y) and x (e_x) axes, respectively:

$$M_x = e_y \times P \tag{12}$$

$$M_y = e_x \times P \tag{13}$$

Tables A.1 and A.2 of Appendix A list the element slenderness ratios about the minor-axis (λ_y) and the web slenderness ratios (h/t) for the selected beam–column elements and compares their strength predicted by the detailed FE models (P_{FE}) and the code-prescribed interaction equation (P_{Code}).

Fig. 19 illustrates the whole data points in comparison with the code-prescribed interaction surface in the normalised 3D $P - M_x - M_y$ space. It can be seen that regardless of the imposed bending moment direction, the interaction equation may provide unsafe strength predictions for the elements with low slenderness ratios ($\lambda_y \leq 50$) by up to 37.2%. On the contrary, the capacities of the beam–columns with medium and high slenderness ratios ($\lambda_y > 50$) were generally underestimated (up to 41.1%) by the code-proposed interaction equation in AISI S100 [20] and AS/NZS 4600 [21] (see Fig. 20).

5.3.2. European design standard

To evaluate the accuracy of the EC3 [28] design guidelines in predicting the strength of CFS beam–column elements, the capacity results obtained using the experimentally validated FE models (P_{FE}) were compared to those predicted by the EC3 interaction equations (Eqs. (6) and (7)) (P_{EC3}). To exclude the inaccuracies associated with the effective width method (EWM), the nominal pure capacities were

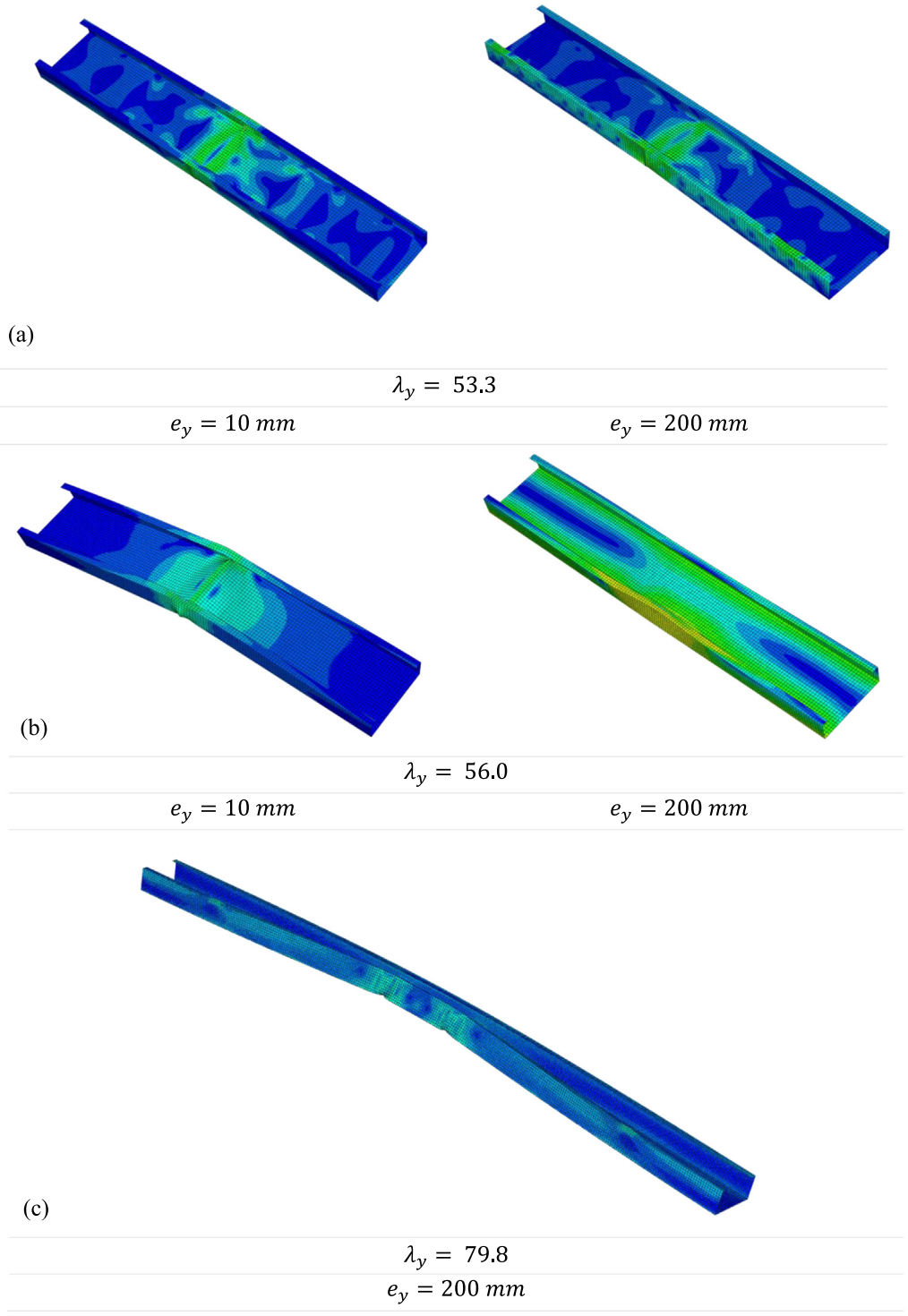

Fig. 13. Failure modes of CFS beam–columns with medium slenderness ratio ($50 < \lambda_y \leq 100$) subjected to combined compression and major-axis bending actions.

obtained using the experimentally validated FE models described in Section 3 (see columns 4 and 5 of Table 5). Since the terms ($\chi_x N_{c,Rd}$) and ($\chi_{LT} M_{cx,Rd}$) in Eqs. (6) and (7) represent the strength of the CFS member under pure compression and pure bending moment about major axis, they were replaced with P_n and M_{nx}, respectively. The term $M_{cy,Rd}$ in Eqs. (6) and (7) represents the cross-sectional capacity of the element under minor axis bending moment. To estimate $M_{cy,Rd}$ using FE models [33], a similar model as those used for the prediction of P_n and M_{nx} was developed, except that the CFS element remained laterally restrained along the web–flange junctions, while equal and opposite minor axis rotations were applied to both ends of the element. Furthermore, the element length was taken as five times the local buckling half-wavelength or three times the distortional buckling half-wavelength, as suggested by Shifferaw and Schafer [44]. The half-wavelength was calculated using the CUFSM [39] software.

Tables A.1 and A.2 of Appendix A list the strength values of the CFS beam–columns obtained using the EC3 [28] interaction equation (P_{EC3}). It can be seen that there is a good agreement between the strength of CFS beam–columns with low slenderness ($\lambda_y \leq 50$) and those obtained from the validated FE models with an average error of 9.2%. On the other hand, EC3 [28] strength predictions for medium

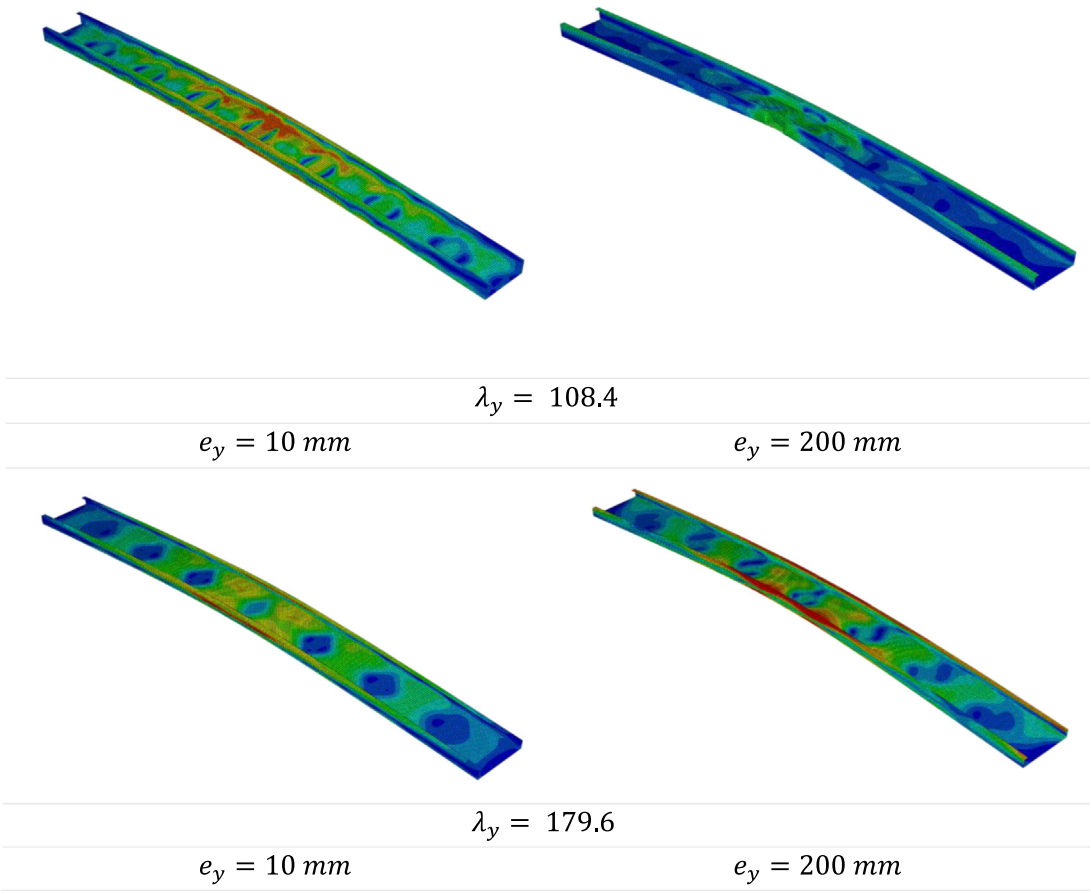

Fig. 14. Failure modes of CFS beam–columns with high slenderness ratio ($\lambda_y > 100$) subjected to combined compression and major-axis bending actions.

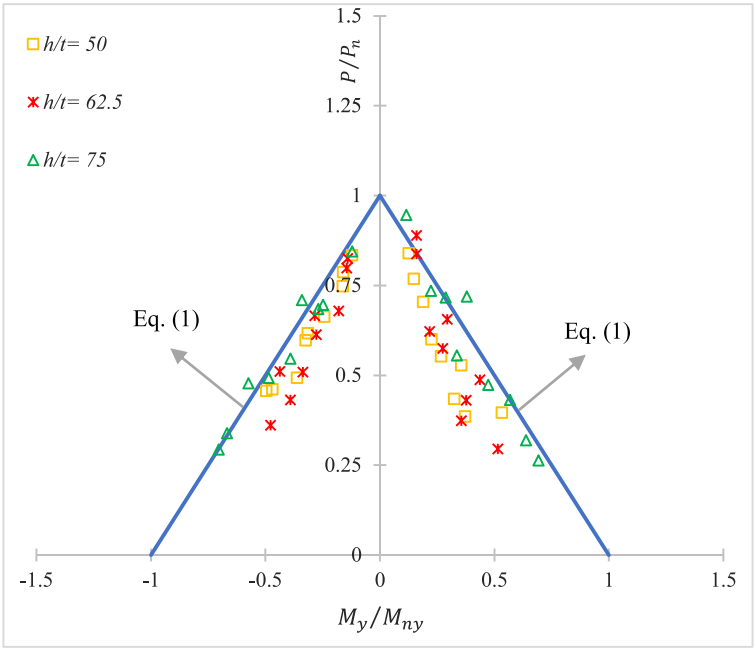

Fig. 15. Interaction of P/P_n and M_y/M_{ny} for CFS beam–columns with low web slenderness ratio ($h/t < 100$).

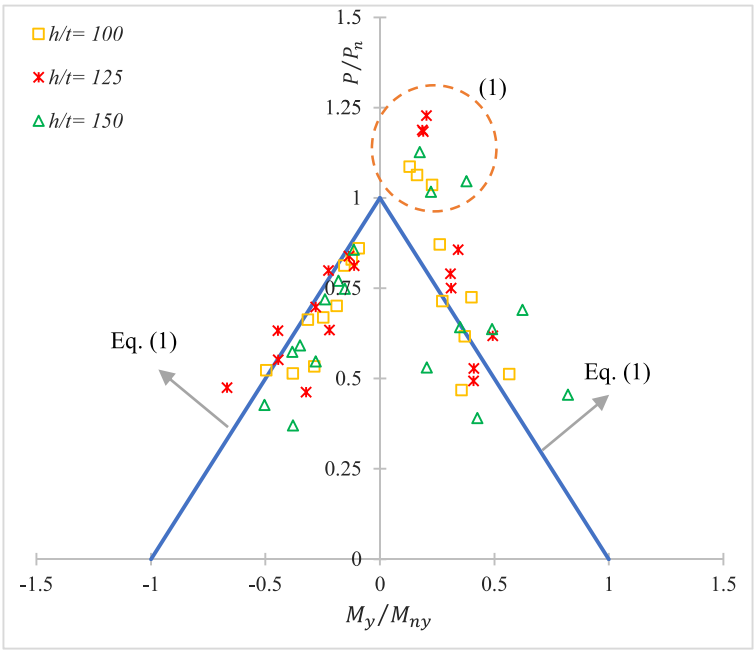

Fig. 16. Interaction of P/P_n and M_y/M_{ny} for CFS beam–columns with medium web slenderness ratio ($100 \leq h/t < 200$).

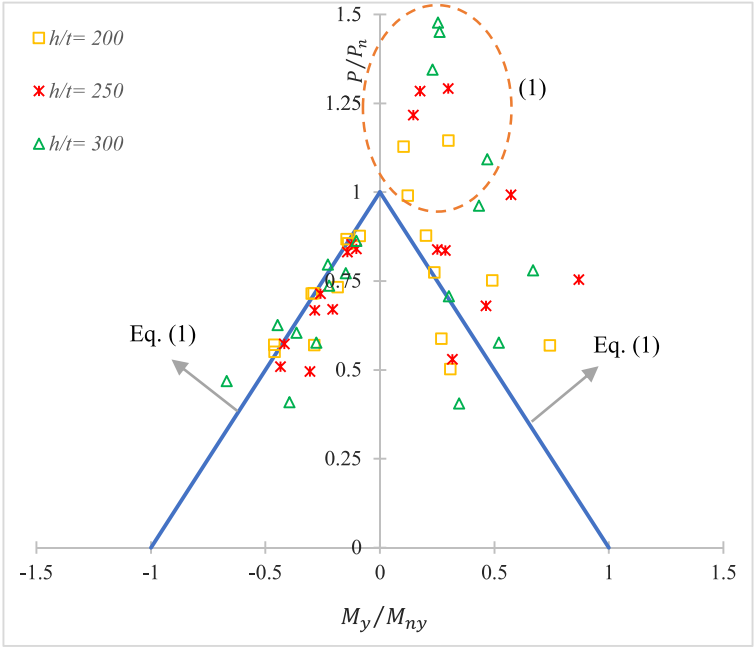

Fig. 17. Interaction of P/P_n and M_y/M_{ny} for CFS beam–columns with high web slenderness ratio ($h/t \geq 200$).

to high slenderness elements ($\lambda_y > 50$) resulted in an average error of 15.6% compared to the FE results.

5.4. Development of a more accurate interaction equation

To improve the strength predictions of the CFS beam–columns, a general trinomial expansion representing curved surfaces was proposed for the interaction equation by taking into account the effects of the element slenderness ratio (λ_y) and web slenderness ratio (h/t) as the key parameters identified in the previous sections. It is worth noting that the effects of these parameters on the behaviour of the beam–columns have not been considered in the code-proposed equations as well as in the literature.

$$\left(\frac{P}{P_n}\right)^{\alpha} + \left(\frac{M_x}{M_{nx}}\right)^{\alpha} + \left(\frac{M_y}{M_{ny}}\right)^{\alpha} \leq 1.0 \tag{14}$$

where

$$\begin{cases} \alpha = 0.95 & For\ \lambda_y \leq 50\ (low\ slenderness) \\ \alpha = 1 + \frac{h/t}{1000} & For\ \lambda_y > 50\ (medium/high\ slenderness) \end{cases} \tag{15}$$

Using an iterative optimisation process, the factor α was obtained for low, medium and high slenderness elements by minimising the errors between the strength results obtained from the proposed equation (P_{Prop}) and the detailed FE models (P_{FE}) calculated by the following

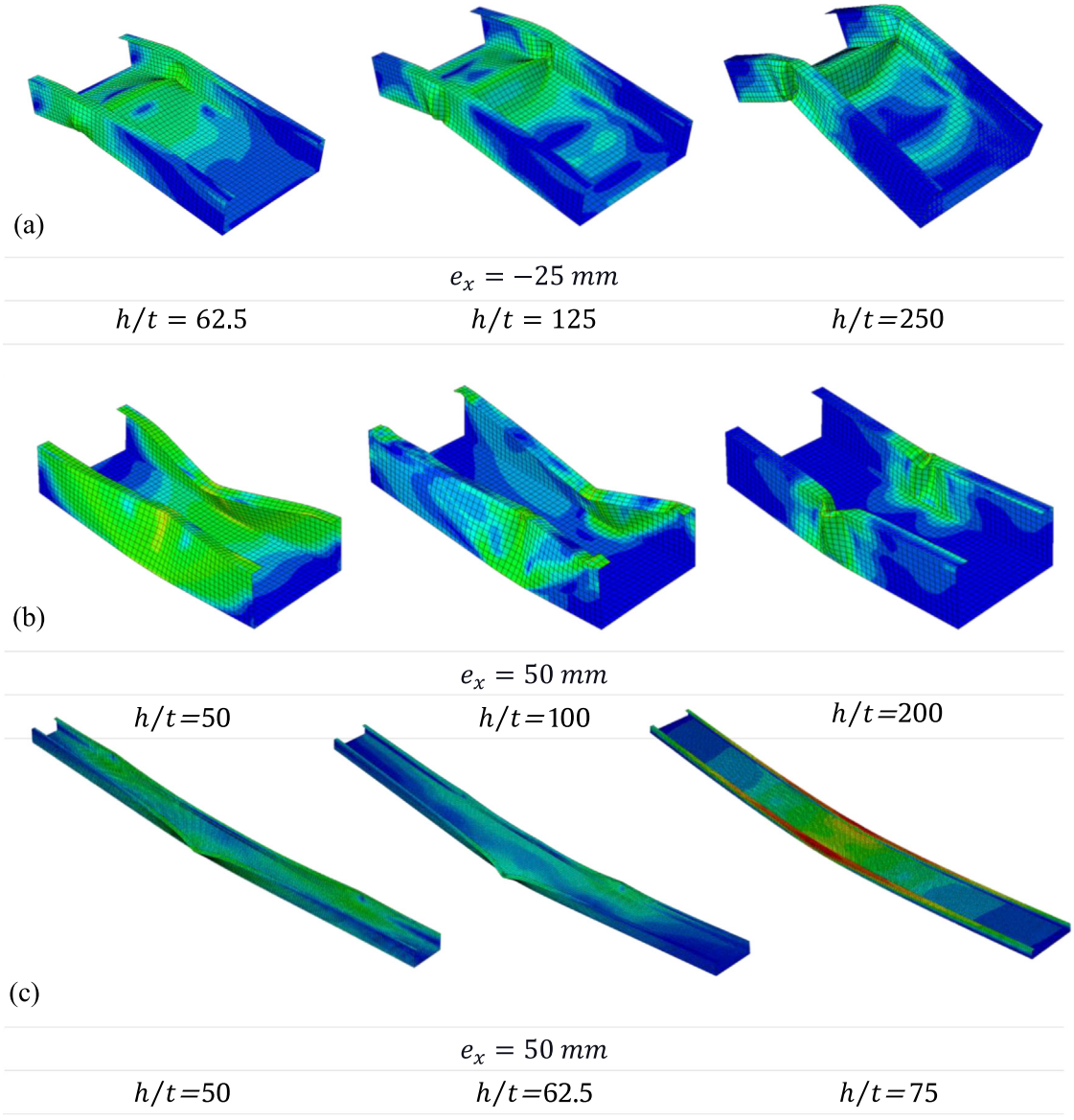

Fig. 18. Failure modes of CFS beam–columns subjected to combined compression and minor-axis bending.

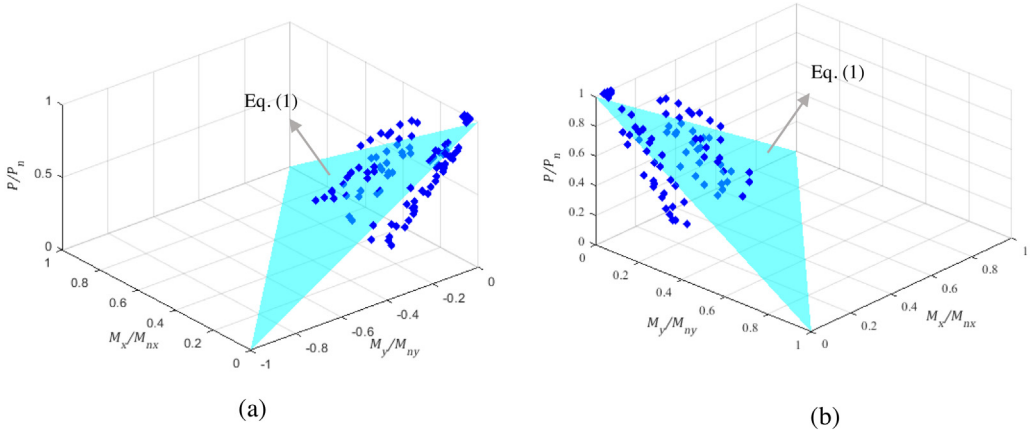

Fig. 19. Normalised FE results and interaction surface for CFS beam–columns with $\lambda_y \leq 50$ under: (a) negative M_y (web in compression) and (b) positive M_y (web in tension).

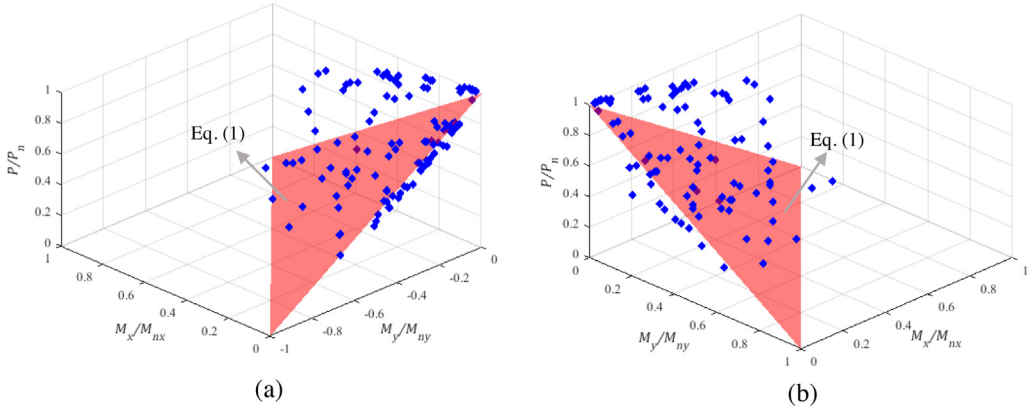

Fig. 20. Normalised FE results and interaction surface for CFS beam–columns with $\lambda_y > 50$ under: (a) negative M_y (web in compression) and (b) positive M_y (web in tension).

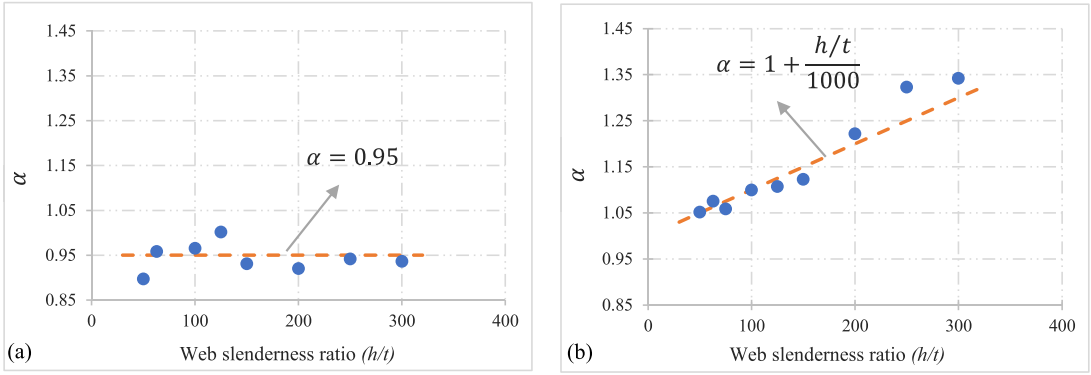

Fig. 21. α factor versus web slenderness ratios for the CFS elements with (a) $\lambda_y \leq 50$ and (b) $\lambda_y > 50$.

equation:

$$Error = \Sigma \left(1 - \frac{P_{prop}}{P_{FE}}\right)^2 \tag{16}$$

The data points were divided into various categories in terms of element slenderness ratio about the minor-axis ($\lambda_y = KL/r_y$) and cross-sectional web slenderness ratio (h/t) to find the best correlation between the actual and the predicted values. The optimum results of the different categories led to the most efficient α variable for Eq. (14) as illustrated in Fig. 21. The presented results are the average α values for each category of the λ_y comprising various h/t ratios. The factor α was kept constant for the elements with low slenderness ratios ($\lambda_y \leq 50$) as h/t exhibited a negligible contribution to the α values (see Fig. 21(a)). However, for the other elements with medium and high slenderness ratios ($\lambda_y > 50$), a linear correlation was observed between the calculated α and h/t of the section (see Fig. 21(b)).

It should be noted that the results of pure compressive members were neglected when the proposed equation was derived in order to develop a more accurate interaction equation for beam–column elements. Furthermore, there were a few data points related to the strength of CFS elements under the combined action of compression and minor-axis bending with webs in tension that exceeded their compressive capacity limit (i.e., $\frac{P}{P_n} > 1$). As shown in Figs. 16 and 17, using any interaction equations for such loading conditions results in over-conservative strength predictions. The reason for the higher compressive capacity of these elements than their pure compressive strength was explained in Section 5.2. Therefore, to avoid any divergence, these data points were also excluded in the development of the interaction equation.

To provide a better insight, an optimal data fitting procedure was also applied to the entire data set, and consequently, a value of α = 1.03 was achieved. This indicates that ignoring the member properties leads to a linear interaction equation as suggested by current design specifications (Eq. (1)). However, as discussed before, the efficiency of this equation depends on the member properties (i.e., element and web slenderness ratios) and does not provide accurate strength predictions for some beam–column elements.

The results of P_{Prop} for all the studied beam–column elements are listed in Tables. A1 and A2. For better comparison, Table 6 lists the average errors associated with the strength predictions obtained using the design guidelines outlined in AISI S100 [20] and AS/NZS 4600 [21] (P_{code}) and EC3 [28] (P_{EC3}), as well as the interaction equation proposed in this study (P_{Prop}). The results indicate that the proposed interaction equation, on average, could improve the accuracy of the code strength predictions, especially in the case of medium to high slenderness elements.

For the low-slenderness CFS beam–columns, all design regulations resulted in an almost similar average error of around 9%. The interaction equations prescribed in EC3 [28] (Eqs. (6) and (7)), however, led to more conservative strength values for CFS elements with medium and high slenderness compared to the other methods. In the case of medium to high slenderness beam–columns, the average errors of the interaction equations prescribed by AISI S100 [20] and AS/NZS 4600 [21] (Eq. (1)) and EC3 Part 1–3 [28] (Eqs. (6) and (7)) were reduced from 12.4% and 15.6%, respectively, to less than 10% by using the proposed equation. The results also indicate that the improvement in the accuracy is more evident in the case of CFS elements with medium and high slenderness ratios. This confirms the findings of Sections 5.1 and 5.2 that the prescribed interaction equation by AISI S100 [20] and AS/NZS 4600 [21] underestimate the strength of CFS beam–columns with medium and high slenderness ratios, with the impact being most noticeable in the cross-sections with high slenderness.

Table 5
Nominal strength of the CFS elements under pure actions.

Section name	Length	Thickness	Nominal capacities of the specimens subjected to the pure actions			
			Compression	Major-axis bending	Minor-axis bending (Web in compression)	Minor-axis bending (Web in tension)
	$L(mm)$	$t(mm)$	P_n (kN)	M_{nx} $(kN.m)$	M_{ny} $(kN.m)$	M_{ny} $(kN.m)$
$C1$	500	1	43.3	10.4	2.2	2.5
		2	139.1	30.2	6.8	6.4
		4	393.6	64.8	8.2	7.5
	1500	1	28.6	5.5	1.0	1.6
		2	83.0	26.3	3.5	2.3
		4	224.4	47.2	5.7	5.6
	3000	1	13.9	5.4	1.2	0.8
		2	35.8	12.9	2.7	2.3
		4	77.0	31.3	5.4	6.4
$C2$	500	1	49.9	9.4	4.1	4.2
		2	172.8	29.0	12.4	11.1
		4	487.8	63.6	26.9	25.6
	1500	1	42.1	5.2	2.5	3.1
		2	132.7	29.9	4.7	8.0
		4	477.3	65.4	18.0	13.7
	3000	1	27.4	4.7	1.9	1.2
		2	76.1	26.3	4.7	4.8
		4	189.5	42.4	11.1	10.6
$C3$	500	1	53.5	8.3	5.3	5.8
		2	195.5	25.0	18.2	16.2
		4	574.5	71.9	39.1	38.4
	1500	1	50.0	7.5	3.0	4.1
		2	174.8	24.9	11.8	11.4
		4	520.2	65.5	25.5	26.9
	3000	1	39.9	3.8	2.5	1.5
		2	128.2	13.2	6.7	5.8
		4	374.4	35.9	17.2	13.9

Table 6
Average error (%) associated with strength predictions of each method compared to the FE results.

Member slenderness ratio	P_{code} vs P_{FE}	P_{EC3} vs P_{FE}	P_{Prop} vs P_{FE}
$\lambda_y \leq 50$	9.4	9.2	9.0
$\lambda_y > 50$	12.4	15.6	9.8

5.5. Accuracy of the proposed equation for NZ sections

The accuracy of the proposed equation was further investigated for standard CFS lipped channel cross-sections utilised in New Zealand (NZ). These elements were chosen due to their various cross-sectional sizes and significantly thinner thicknesses than those of the elements used to develop the interaction equation. In total, 180 new CFS beam–columns were examined under 15 different eccentricities, by considering two sets of cross-sectional dimensions ($CN1$ and $CN2$), three thicknesses (0.75 *mm*, 0.95 *mm*, and 1.15 *mm*) and two element lengths (1500 *mm* and 3000 *mm*), as shown in Table 7. The strength values derived from the proposed equation (P_{Prop}) were compared to those obtained from the FE models (P_{FE}) and the interaction equation (P_{Code}) recommended by the AISI S100 [20] and AS/NZS 4600 [21], as listed in Table A.3 of Appendix A. It should be noted that the FE modelling techniques outlined in Section 3 were replicated herein to predict the strength of the selected beam–columns with the NZ sections. By comparing the results of P_{Prop}/P_{FE} and P_{Code}/P_{FE}, it can be concluded that using the proposed equation could improve the accuracy of the code-prescribed interaction equation (Eq. (1)) predictions on average by 14%.

6. Reliability analysis

A reliability analysis was conducted within the framework of the AISI S100 [45] to ensure that the proposed design equation (Eq. (14)) provides the required level of safety. Design equations were considered reliable if the value of the reliability index (β_0) exceeded the specific target value defined in the AISI S100 [20]. Different sources of uncertainties, such as material properties, dimensions, and the proposed design approaches, are expressed by the Load and Resistance Factor Design as follows [45]:

$$\sum \gamma_i Q_i \leq \varnothing R_n \tag{17}$$

where $\sum \gamma_i Q_i$ is the required strength based on the critical load combination, $\varnothing$ is the resistance factor and R_n is the nominal predicted strength. According to the AISI framework [45], the resistance factor $\varnothing$ is obtained as:

$$\varnothing = C_{\varnothing}(M_m F_m P_{m1} P_{m2}) e^{-\beta_0 \sqrt{V_M^2 + V_F^2 + C_{P1} V_{P1}^2 + C_{P2} V_{P2}^2 + V_Q^2}} \tag{18}$$

where $C_{\varnothing}$ is the calibration factor for LRFD design considered equal to 1.52 [45], and M_m = 1.10 and F_m = 1.00 are the mean values of the material and fabrication factors, respectively. P_{m1} is the mean ratio of the capacity obtained by FE analysis to the capacity estimated by the proposed design equation (i.e., P_{FE}/P_{Prop}) and P_{m2} is the mean ratio of the experimentally predicted capacity to the corresponding FE result (i.e., P_{Test}/P_{FE} in the validated models). The factor β_0 is the target

Table 7
Features of CFS beam–columns with standard NZ lipped channel sections.

Section name	Web height	Flange	Lip	Radius of round corners	Thickness	Length
	h (mm)	b_f (mm)	d_1(mm)	R (mm)	t (mm)	L (mm)
$CN1$	89	40	11	2	0.75, 0.95 and 1.15	1500 and 3000
$CN2$	152	64	14.5	2		

Table 8
Selected factors for the reliability analysis based on the AISI.

Variable	P_{m1}	P_{m2}	V_{p1}	V_{p2}	C_{p1}	C_{p2}
Magnitude	1.048	0.992	0.154	0.020	1.007	1.481

reliability index assumed to be 2.5 for structural members. V_m = 0.10 and V_F = 0.05 are the coefficient of variations for the material and fabrication factors, respectively. The products of V_{p1} and V_{p2} are the coefficient of variations (COV) of P_{m1} and P_{m2}, respectively, and V_Q = 0.21 is coefficient of variation of the loading [45]. Lastly, C_p is the correction factor accounting for the number of tested specimens (n), calculated according to the following equation:

$$C_p = \frac{n+1}{n}\frac{n-1}{n-3} \tag{19}$$

The factor C_{p1} is determined by the number of FE models, which in this case is 405 for the CFS elements under combined compressive and bending actions. The factor C_{p2} is determined by the number of experimental samples in the validation procedure, taken equal to nine in this study. The selected values for all the above-mentioned factors are summarised in Table 8.

The resistance factor (∅) for the proposed interaction equation (Eq. (14)) was obtained equal to 0.854, which exceeds the safety factor of 0.85 prescribed by the AISI [45] design rules for the CFS members subjected to the combined axial compression and bending. This indicates that the proposed interaction equation can be considered reliable for practical applications.

7. Summary and conclusion

This paper aimed to improve the accuracy of the linear interaction equations recommended by AISI S100 [20] and AS/NZS 4600 [21] for the design of CFS single section beam–column elements. For this purpose, experimentally validated FE models of CFS beam–columns taking into account the geometric imperfections and the material nonlinearity were employed to conduct a comprehensive parametric study. The developed dataset comprised a wide range of key design parameters, including different cross-sectional geometries, lengths as well as directions and values of load eccentricities to study various combinations of axial compression and bending moments about minor- and major-axes. The results were then used to assess the accuracy of current design specifications, including AISI S100 [20], AS/NZS 4600 [21] and EC3 [28] to predict the load-carrying capacity of CFS beam–column elements. Subsequently, by minimising the errors between the strength results obtained from the validated FE models and the predicted values using an iterative optimisation method, a general trinomial expansion was proposed for the interaction equation, as a function of element and web slenderness ratios. Based on the presented results, the following conclusions were drawn:

- The crucial factors affecting the behaviour of CFS cross-sections subjected to the combined action of compression and major-axis bending were the element slenderness ratio (λ_y), the eccentricity magnitude and the thickness of the specimens.
- For the CFS elements subjected to the combined compression and minor-axis bending, the web slenderness ratio (h/t) and the sign of the eccentricity were the most important parameters affecting their behaviour.
- The accuracy of the interaction equations specified in the design codes, in general, is influenced by the following three main factors: (i) element slenderness ratio (λ_y), (ii) web slenderness ratio (h/t) and (iii) the value and direction of the eccentricities (e_y and e_x).
- For low-slenderness CFS beam–column elements ($\lambda_y \leq 50$), the current design regulations resulted in an almost similar average error of around 9%. In the case of medium to high slenderness elements ($\lambda_y > 50$), however, the EC3 interaction equations [28] provided the most conservative predictions with the average error of 15.6%.
- For CFS beam–column elements with low slenderness ratios ($\lambda_y \leq 50$), the α factor for the proposed interaction equation is almost similar to the prescribed interaction equations in AISI S100 [20] and AS/NZS 4600 [21]. However, in the case of medium to high slenderness ($\lambda_y > 50$) elements, the average errors of AISI S100 [20] and AS/NZS 4600 [21] (Eq. (1)) and EC3 Part 1–3 [28] (Eqs. (6) and (7)) predictions were reduced from 12.4% and 15.6%, respectively, to 9.8% by using the proposed equation.
- The accuracy of the proposed equation was also highlighted for the prediction of the compression capacities of standard CFS lipped channel cross-sections utilised in NZ. Finally, the results of a reliability analysis, conducted within the framework of the AISI, demonstrated that the proposed design equation is reliable for use in practical design.

CRediT authorship contribution statement

Maryam Hasanali: Writing – original draft, Visualization, Validation, Software, Resources, Project administration, Methodology, Investigation, Formal analysis, Data curation, Conceptualization. **Seyed Mohammad Mojtabaei:** Writing – original draft, Validation, Supervision, Conceptualization. **Iman Hajirasouliha:** Writing – review & editing, Validation, Supervision, Methodology, Conceptualization. **G. Charles Clifton:** Writing – review & editing, Validation, Supervision. **James B.P. Lim:** Writing – review & editing, Validation, Supervision.

Declaration of competing interest

The authors declare that they have no known competing financial interests or personal relationships that could have appeared to influence the work reported in this paper.

Data availability

Data will be made available on request.

Acknowledgements

The first author would like to acknowledge gratefully the University of Auckland, New Zealand for providing financial support through a University of Auckland Doctoral Scholarship.

Appendix

See Tables A.1–A.3.

Table A.1
Comparison between the strength of CFS beam–columns obtained using FE analysis (P_{FE}), code-prescribed interaction equations (P_{code}) and (P_{EC3}) as well as proposed interaction equation (P_{Prop}) for elements with $\lambda_y \leq 50$.

Length	Web height	Thickness	Element slenderness ratio	Web slenderness ratio	Eccentricities		Capacity				Ratio			Error (%)		
L (mm)	h (mm)	t (mm)	λ_y	h/t	e_y (mm)	e_x (mm)	P_{FE} (kN)	P_{Code} (kN)	P_{EC3} (kN)	P_{Prop} (kN)	$\frac{P_{Code}}{P_{FE}}$	$\frac{P_{EC3}}{P_{FE}}$	$\frac{P_{Prop}}{P_{FE}}$	$\frac{P_{Code}}{P_{FE}}$ vs	$\frac{P_{EC3}}{P_{FE}}$ vs	$\frac{P_{Prop}}{P_{FE}}$ vs
500	200	1	13.1	200	0	−10	46.9	48.6	47.7	47.8	1.04	1.02	1.04	3.62	1.79	1.91
					0	25	46.9	43.5	39.1	42.4	0.93	0.83	0.90	7.31	16.68	9.66
					0	−25	39.2	42.7	41.0	41.6	1.09	1.05	1.06	9.00	4.73	6.11
					0	50	31.4	36.7	30.8	35.5	1.17	0.98	1.13	16.70	1.97	12.92
					0	−50	30.5	35.6	33.3	34.4	1.17	1.09	1.13	16.75	9.26	12.88
					10	0	52.8	50.2	50.3	49.6	0.95	0.95	0.94	4.80	4.72	5.99
					100	0	30.4	32.5	32.5	31.4	1.07	1.07	1.03	7.02	7.03	3.30
					200	0	20.3	23.4	23.4	22.5	1.15	1.15	1.11	15.35	15.33	11.27
					10	−10	46.3	45.9	45.1	44.6	0.99	0.97	0.96	0.87	2.53	3.55
					100	25	30.0	28.6	26.6	27.1	0.95	0.89	0.90	4.83	11.41	9.54
					100	−25	26.9	28.2	27.5	26.8	1.05	1.02	1.00	4.83	2.04	0.42
					200	50	18.8	19.5	17.7	18.5	1.04	0.94	0.98	3.66	5.91	1.78
					200	−50	17.6	19.2	18.5	18.1	1.09	1.05	1.03	8.76	4.83	2.98
500	200	2	13.3	100	0	−10	168.1	176.5	167.5	173.5	1.05	1.00	1.03	4.99	0.35	3.18
					0	25	170.1	150.2	134.6	146.0	0.88	0.79	0.86	11.66	20.86	14.17
					0	−25	136.9	154.1	137.9	149.9	1.13	1.01	1.09	12.54	0.72	9.49
					0	50	120.4	122.0	102.6	117.8	1.01	0.85	0.98	1.33	14.78	2.14
					0	−50	104.1	127.2	106.5	122.9	1.22	1.02	1.18	22.10	2.27	18.00
					10	0	191.8	181.2	181.3	178.7	0.95	0.95	0.93	5.49	5.45	6.83
					100	0	106.9	109.6	109.7	105.7	1.03	1.03	0.99	2.56	2.66	1.08
					200	0	70.7	76.1	76.2	73.5	1.08	1.08	1.04	7.73	7.87	3.99
					10	−10	165.6	164.8	157.0	160.0	1.00	0.95	0.97	0.45	5.18	3.34
					100	25	97.8	93.8	87.5	88.9	0.96	0.89	0.91	4.09	10.51	9.02
					100	−25	97.2	95.3	88.9	90.4	0.98	0.91	0.93	2.01	8.57	6.98
					200	50	59.6	61.7	56.4	58.4	1.03	0.95	0.98	3.44	5.50	2.02
					200	−50	63.0	63.0	57.5	59.7	1.00	0.91	0.95	0.01	8.67	5.20
500	200	4	13.6	50	0	10	481.7	499.6	462.4	489.3	1.04	0.96	1.02	3.72	4.02	1.57
					0	−10	478.7	500.9	468.1	490.7	1.05	0.98	1.03	4.65	2.21	2.51
					0	25	344.4	418.0	359.2	405.2	1.21	1.04	1.18	21.35	4.29	17.63
					0	−25	380.8	420.3	367.9	407.5	1.10	0.97	1.07	10.35	3.40	7.00
					0	50	249.2	328.5	262.4	316.9	1.32	1.05	1.27	31.80	5.27	27.15
					0	−50	283.0	331.3	271.7	319.6	1.17	0.96	1.13	17.06	4.02	12.93
					10	0	568.7	531.9	529.8	524.3	0.94	0.93	0.92	6.47	6.84	7.82
					100	0	286.3	319.3	316.0	307.9	1.12	1.10	1.08	11.53	10.39	7.57
					200	0	183.7	221.1	218.9	213.4	1.20	1.19	1.16	20.33	19.15	16.18
					10	10	475.3	467.2	432.9	452.2	0.98	0.91	0.95	1.71	8.92	4.86
					10	−10	473.4	468.3	437.9	453.3	0.99	0.93	0.96	1.08	7.50	4.24
					100	25	247.1	264.3	237.2	250.3	1.07	0.96	1.01	6.95	4.00	1.30
					100	−25	293.7	265.2	241.0	251.2	0.90	0.82	0.86	9.70	17.94	14.46
					200	50	150.1	171.6	150.1	162.4	1.14	1.00	1.08	14.31	0.02	8.15
					200	−50	179.6	172.4	153.1	163.1	0.96	0.85	0.91	4.02	14.74	9.18
500	250	1	17.8	250	0	−10	42.0	44.4	43.0	43.6	1.06	1.02	1.04	5.82	2.40	3.85
					0	25	41.9	38.5	34.2	37.4	0.92	0.82	0.89	8.14	18.20	10.74
					0	−25	33.5	38.2	35.6	37.1	1.14	1.06	1.11	14.01	6.41	10.74
					0	50	26.5	31.3	26.1	30.2	1.18	0.98	1.14	18.13	1.55	14.08
					0	−50	24.8	30.9	27.7	29.8	1.25	1.12	1.20	24.64	11.74	20.34
					10	0	49.5	47.4	47.4	46.9	0.96	0.96	0.95	4.20	4.22	5.25
					100	0	33.1	32.6	32.6	31.5	0.99	0.99	0.95	1.39	1.37	4.70
					200	0	22.8	24.2	24.2	23.3	1.06	1.06	1.02	5.90	5.94	2.11

(*continued on next page*)

Table A.1 (*continued*).

					10	−10	41.5	42.4	41.1	41.3	1.02	0.99	0.99	2.14	1.01	0.68
					100	25	30.8	27.3	25.1	25.9	0.89	0.82	0.84	11.35	18.44	15.86
					100	−25	26.5	27.1	25.8	25.7	1.02	0.98	0.97	2.45	2.47	2.77
					200	50	18.7	18.8	16.8	17.7	1.01	0.90	0.95	0.65	10.10	4.87
					200	−50	17.5	18.6	17.4	17.6	1.07	1.00	1.01	6.53	0.36	0.68
					0	−10	140.2	151.6	142.1	148.6	1.08	1.01	1.06	8.09	1.33	5.93
					0	25	136.5	124.4	109.0	120.5	0.91	0.80	0.88	8.88	20.16	11.70
					0	−25	109.5	128.0	112.2	124.2	1.17	1.02	1.13	16.96	2.49	13.46
					0	50	91.1	97.2	79.6	93.7	1.07	0.87	1.03	6.69	12.62	2.91
					0	−50	79.9	101.7	83.1	98.2	1.27	1.04	1.23	27.33	3.99	22.87
					10	0	172.4	163.0	163.1	161.1	0.95	0.95	0.93	5.45	5.42	6.57
500	250	2	18.1	125	100	0	120.0	108.2	108.3	104.5	0.90	0.90	0.87	9.79	9.75	12.88
					200	0	82.9	78.8	78.8	76.0	0.95	0.95	0.92	4.91	4.86	8.30
					10	−10	139.8	144.1	135.5	139.8	1.03	0.97	1.00	3.06	3.09	0.01
					100	25	106.7	87.0	79.2	82.4	0.82	0.74	0.77	18.43	25.75	22.73
					100	−25	94.0	88.8	80.9	84.2	0.95	0.86	0.90	5.48	13.89	10.40
					200	50	65.3	58.2	51.4	54.9	0.89	0.79	0.84	10.92	21.30	15.86
					200	−50	59.5	59.8	52.8	56.5	1.00	0.89	0.95	0.36	11.31	5.17
					0	10	408.2	409.6	375.2	400.1	1.00	0.92	0.98	0.35	8.09	1.99
					0	−10	389.0	412.8	381.9	403.3	1.06	0.98	1.04	6.10	1.84	3.68
					0	25	280.2	330.3	279.9	319.5	1.18	1.00	1.14	17.87	0.10	14.02
					0	−25	298.9	335.4	289.3	324.6	1.12	0.97	1.09	12.21	3.21	8.59
					0	50	182.0	249.7	197.1	240.8	1.37	1.08	1.32	37.19	8.27	32.28
					0	−50	210.1	255.6	206.4	246.5	1.22	0.98	1.17	21.65	1.75	17.29
					10	0	485.3	453.0	451.4	446.7	0.93	0.93	0.92	6.65	6.99	7.96
500	250	4	18.7	63	100	0	296.7	276.1	273.4	266.3	0.93	0.92	0.90	6.96	7.87	10.26
					200	0	198.7	192.5	190.7	185.8	0.97	0.96	0.94	3.10	4.02	6.47
					10	10	406.8	384.9	353.2	371.8	0.95	0.87	0.91	5.39	13.18	8.61
					10	−10	388.5	387.6	359.1	374.6	1.00	0.92	0.96	0.24	7.57	3.59
					100	25	236.9	217.4	192.7	205.6	0.92	0.81	0.87	8.23	18.67	13.20
					100	−25	249.9	219.6	197.1	207.8	0.88	0.79	0.83	12.10	21.11	16.84
					200	50	146.5	139.9	120.5	132.2	0.96	0.82	0.90	4.49	17.71	9.74
					200	−50	151.8	141.7	124.0	133.9	0.93	0.82	0.88	6.62	18.29	11.74
					0	−10	33.4	36.3	35.0	35.4	1.08	1.05	1.06	8.46	4.73	5.91
					0	25	30.6	30.3	27.3	29.4	0.99	0.89	0.96	0.88	10.77	4.03
					0	−25	25.0	29.2	27.3	28.2	1.17	1.09	1.13	16.91	9.45	13.08
					0	50	17.6	23.4	20.0	22.5	1.33	1.14	1.28	32.97	13.99	28.23
					0	−50	17.7	22.0	20.0	21.2	1.24	1.13	1.20	24.30	13.11	19.84
					10	0	43.1	41.5	41.5	41.1	0.96	0.96	0.96	3.53	3.69	4.43
500	300	1	27.8	300	100	0	33.5	30.6	30.3	29.6	0.91	0.90	0.88	8.74	9.59	11.62
					200	0	25.1	23.6	23.4	22.8	0.94	0.93	0.91	5.71	6.77	9.07
					10	−10	33.3	35.0	33.8	34.0	1.05	1.01	1.02	5.21	1.47	1.99
					100	25	29.7	23.5	21.5	22.3	0.79	0.72	0.75	20.98	27.84	25.07
					100	−25	22.6	22.8	21.5	21.6	1.01	0.95	0.96	0.92	4.99	4.37
					200	50	15.7	16.1	14.3	15.2	1.03	0.91	0.97	2.68	8.81	3.07
					200	−50	14.8	15.5	14.3	14.6	1.04	0.97	0.98	4.24	3.49	1.61
					0	−10	104.1	115.4	105.8	112.6	1.11	1.02	1.08	10.79	1.61	8.11
					0	25	89.3	90.0	75.5	87.0	1.01	0.84	0.97	0.79	15.51	2.61
					0	−25	76.2	91.9	78.8	88.8	1.21	1.03	1.17	20.60	3.41	16.59
					0	50	54.3	66.6	52.3	64.2	1.23	0.96	1.18	22.54	3.68	18.15

(*continued on next page*)

Table A.1 (*continued*).

500	300	2	28.5	150	0	−50	51.5	68.6	55.5	66.1	1.33	1.08	1.28	33.25	7.84	28.48
					10	0	139.1	133.0	132.1	131.7	0.96	0.95	0.95	4.38	5.04	5.34
					100	0	106.5	95.2	93.1	92.1	0.89	0.87	0.86	10.61	12.60	13.51
					200	0	78.1	72.4	70.6	69.8	0.93	0.90	0.89	7.36	9.64	10.68
					10	−10	103.9	111.1	101.7	107.6	1.07	0.98	1.04	7.00	2.12	3.60
					100	25	80.7	69.3	59.3	65.6	0.86	0.73	0.81	14.08	26.54	18.66
					100	−25	69.1	70.4	61.3	66.7	1.02	0.89	0.97	1.97	11.22	3.45
					200	50	48.8	46.2	38.1	43.6	0.95	0.78	0.89	5.36	22.02	10.67
					200	−50	43.1	47.1	39.7	44.5	1.09	0.92	1.03	9.36	7.85	3.22
1500	200	1	39.4	200	0	10	49.5	44.6	34.2	43.7	0.90	0.69	0.88	10.04	30.90	11.71
					0	−10	43.4	42.9	36.3	41.9	0.99	0.84	0.97	1.26	16.46	3.42
					0	25	38.8	38.3	28.9	37.2	0.99	0.75	0.96	1.21	25.38	4.03
					0	−25	35.8	35.3	32.3	34.2	0.99	0.90	0.96	1.31	9.76	4.42
					0	50	25.2	31.0	23.2	29.9	1.23	0.92	1.19	23.32	7.75	19.08
					0	−50	27.6	27.3	27.3	26.3	0.99	0.99	0.95	1.03	1.03	4.56
					10	0	47.6	46.9	36.7	46.3	0.98	0.77	0.97	1.51	23.03	2.77
					100	0	26.9	30.1	23.5	29.0	1.12	0.87	1.08	11.67	12.77	7.78
					200	0	17.1	21.5	17.1	20.7	1.26	1.00	1.21	25.90	0.21	21.45
					10	10	45.5	42.1	32.1	40.9	0.93	0.71	0.90	7.43	29.48	10.11
					10	−10	42.5	40.6	33.8	39.3	0.95	0.80	0.92	4.56	20.38	7.60
					100	25	21.4	25.4	19.3	24.1	1.19	0.90	1.13	18.90	9.70	12.78
					100	−25	25.2	24.0	20.7	22.8	0.96	0.82	0.90	4.45	17.65	9.55
					200	50	13.7	17.0	13.1	16.1	1.24	0.96	1.18	24.40	4.12	17.68
					200	−50	16.4	15.8	14.3	15.0	0.97	0.88	0.91	3.29	12.47	8.64
1500	200	2	39.9	100	0	−10	144.9	152.2	141.2	149.1	1.05	0.97	1.03	5.09	2.51	2.93
					0	25	124.8	126.5	111.7	122.6	1.01	0.90	0.98	1.37	10.49	1.75
					0	−25	116.9	127.6	114.5	123.7	1.09	0.98	1.06	9.11	2.07	5.78
					0	50	81.7	99.1	85.6	95.6	1.21	1.05	1.17	21.24	4.69	16.95
					0	−50	89.7	100.4	88.7	96.9	1.12	0.99	1.08	11.96	1.13	8.01
					10	0	172.7	163.3	155.5	161.2	0.95	0.90	0.93	5.45	9.98	6.70
					100	0	104.0	102.7	91.1	99.1	0.99	0.88	0.95	1.25	12.45	4.72
					200	0	67.3	72.7	64.5	70.2	1.08	0.96	1.04	8.17	4.13	4.36
					10	−10	143.6	143.5	128.0	139.0	1.00	0.89	0.97	0.05	10.83	3.16
					100	25	85.1	83.9	69.0	79.5	0.99	0.81	0.93	1.42	18.93	6.64
					100	−25	89.8	84.4	70.1	79.9	0.94	0.78	0.89	6.00	21.86	10.96
					200	50	51.5	55.2	45.0	52.2	1.07	0.87	1.01	7.08	12.72	1.22
					200	−50	58.9	55.6	45.9	52.6	0.94	0.78	0.89	5.56	22.00	10.71
1500	200	4	40.8	50	0	10	399.5	435.8	393.9	425.6	1.09	0.99	1.07	9.09	1.41	6.52
					0	−10	409.0	431.9	399.2	421.5	1.06	0.98	1.03	5.59	2.40	3.04
					0	25	287.4	350.5	303.4	339.0	1.22	1.06	1.18	21.97	5.57	17.96
					0	−25	320.7	344.3	310.7	332.8	1.07	0.97	1.04	7.36	3.11	3.80
					0	50	200.2	264.3	223.8	254.9	1.32	1.12	1.27	32.03	11.81	27.30
					0	−50	239.4	257.3	231.4	248.1	1.07	0.97	1.04	7.45	3.36	3.61
					10	0	513.1	481.9	457.1	475.0	0.94	0.89	0.93	6.07	10.90	7.41
					100	0	264.6	289.9	256.8	279.6	1.10	0.97	1.06	9.56	2.96	5.67
					200	0	171.2	201.0	178.5	194.0	1.17	1.04	1.13	17.37	4.27	13.32
					10	10	395.8	408.6	355.2	394.6	1.03	0.90	1.00	3.24	10.25	0.32
					10	−10	406.4	405.2	359.7	391.0	1.00	0.89	0.96	0.29	11.49	3.77
					100	25	197.5	228.3	185.4	215.9	1.16	0.94	1.09	15.60	6.13	9.33
					100	−25	255.2	225.7	188.3	213.4	0.88	0.74	0.84	11.58	26.21	16.40
					200	50	120.5	146.3	118.0	138.2	1.21	0.98	1.15	21.37	2.11	14.71
					200	−50	158.5	144.1	120.2	136.2	0.91	0.76	0.86	9.11	24.15	14.11
					Average						**1.04**	**0.94**	**1.00**	**9.36**	**9.15**	**9.03**

Table A.2
Comparison between the strength of CFS beam–columns obtained using FE analysis (P_{FE}), code-prescribed interaction equations (P_{Code}) and (P_{EC3}) as well as proposed interaction equation (P_{Prop}) for elements with $\lambda_y > 50$.

Length	Web height	Thickness	Element slenderness ratio	Web slenderness ratio	Eccentricities		Capacity				Ratio			Error (%)		
L (mm)	h (mm)	t (mm)	λ_y	h/t	e_y (mm)	e_x (mm)	P_{FE} (kN)	P_{Code} (kN)	P_{EC3} (kN)	P_{Prop} (kN)	$\frac{P_{Code}}{P_{FE}}$	$\frac{P_{EC3}}{P_{FE}}$	$\frac{P_{Prop}}{P_{FE}}$	$\frac{P_{Code}}{P_{FE}}$ vs	$\frac{P_{EC3}}{P_{FE}}$ vs	$\frac{P_{Prop}}{P_{FE}}$ vs
1500	250	1	53.3	250	0	−10	35.0	35.9	35.4	38.7	1.03	1.01	1.11	2.69	1.08	10.61
					0	25	35.2	31.4	28.2	35.0	0.89	0.80	0.99	10.81	19.76	0.63
					0	−25	28.1	29.5	29.3	33.2	1.05	1.04	1.18	4.84	4.29	18.02
					0	50	28.6	25.0	21.9	28.6	0.87	0.76	1.00	12.62	23.68	0.08
					0	−50	21.4	22.7	23.1	26.0	1.06	1.08	1.22	5.90	7.95	21.55
					10	0	41.7	38.9	37.6	40.6	0.93	0.90	0.98	6.72	9.85	2.50
					100	0	30.5	23.2	21.4	26.6	0.76	0.70	0.87	24.01	29.86	12.82
					200	0	22.1	16.0	14.8	18.2	0.73	0.67	0.83	27.50	32.84	17.32
					10	−10	34.7	33.6	32.1	37.5	0.97	0.92	1.08	3.18	7.56	8.18
					100	25	25.1	19.5	16.9	23.8	0.78	0.67	0.95	22.41	32.83	5.25
					100	−25	23.2	18.8	17.3	23.1	0.81	0.74	0.99	19.28	25.57	0.78
					200	50	15.4	12.7	10.9	15.6	0.83	0.71	1.01	17.26	28.91	1.48
					200	−50	15.7	12.1	11.2	14.9	0.77	0.71	0.95	23.30	28.54	5.41
1500	250	2	54.2	125	0	−10	106.0	103.6	105.3	109.6	0.98	0.99	1.03	2.34	0.69	3.36
					0	25	99.6	93.9	81.9	100.3	0.94	0.82	1.01	5.70	17.73	0.74
					0	−25	84.0	77.9	84.1	84.0	0.93	1.00	1.00	7.26	0.18	0.03
					0	50	65.5	72.6	61.8	78.4	1.11	0.94	1.20	10.86	5.61	19.67
					0	−50	62.9	55.1	64.2	59.4	0.88	1.02	0.94	12.45	2.06	5.61
					10	0	132.3	127.1	122.4	129.3	0.96	0.93	0.98	3.96	7.48	2.30
					100	0	103.3	91.9	82.3	98.3	0.89	0.80	0.95	11.04	20.36	4.81
					200	0	76.5	70.3	62.2	75.9	0.92	0.81	0.99	8.13	18.66	0.79
					10	−10	105.7	100.1	98.5	107.3	0.95	0.93	1.01	5.35	6.83	1.45
					100	25	79.2	71.4	58.4	79.8	0.90	0.74	1.01	9.81	26.23	0.78
					100	−25	74.1	61.8	59.6	69.3	0.83	0.80	0.94	16.64	19.56	6.41
					200	50	47.4	48.9	39.2	55.2	1.03	0.83	1.16	3.00	17.30	16.33
					200	−50	49.0	40.2	40.3	45.4	0.82	0.82	0.92	17.94	17.93	7.51
3000	200	1	78.8	200	0	−10	34.2	34.4	34.6	36.6	1.01	1.01	1.07	0.54	1.06	6.89
					0	25	30.0	24.2	28.4	27.0	0.80	0.95	0.90	19.55	5.33	10.10
					0	−25	28.6	28.4	29.8	31.3	1.00	1.04	1.10	0.47	4.12	9.70
					0	50	22.7	17.3	22.9	19.4	0.76	1.01	0.85	23.74	0.94	14.55
					0	−50	22.8	22.1	24.6	24.8	0.97	1.08	1.09	3.05	7.82	8.71
					10	0	38.9	36.2	33.9	37.8	0.93	0.87	0.97	7.02	12.69	2.66
					100	0	20.3	19.5	17.2	21.9	0.96	0.85	1.08	3.96	15.17	7.80
					200	0	11.4	12.9	11.5	14.3	1.13	1.01	1.26	13.39	1.10	25.67
					10	−10	33.8	31.5	29.9	34.8	0.93	0.89	1.03	6.64	11.42	3.08
					100	25	20.3	14.8	14.4	17.7	0.73	0.71	0.87	27.32	29.15	13.07
					100	−25	21.8	16.3	14.8	19.3	0.75	0.68	0.88	25.32	32.21	11.56
					200	50	12.4	9.1	9.2	10.8	0.73	0.74	0.87	26.68	25.65	12.79
					200	−50	12.4	10.2	9.5	12.1	0.83	0.77	0.97	17.35	23.31	2.51
					0	−10	104.1	107.7	108.5	111.9	1.03	1.04	1.08	3.48	4.18	7.53
					0	25	92.9	82.6	89.6	87.6	0.89	0.96	0.94	11.08	3.60	5.69
					0	−25	85.0	86.9	91.4	92.0	1.02	1.08	1.08	2.29	7.63	8.24
					0	50	65.6	61.0	71.5	64.9	0.93	1.09	0.99	7.13	8.99	1.10
					0	−50	67.0	65.7	73.8	70.0	0.98	1.10	1.04	1.90	10.12	4.48

(*continued on next page*)

Table A.2 (*continued*).

					10	0	126.8	116.9	110.1	119.9	0.92	0.87	0.95	7.79	13.13	5.43
3000	200	2	79.8	100	100	0	94.2	65.1	57.5	69.4	0.69	0.61	0.74	30.83	38.89	26.33
					200	0	65.5	43.7	38.9	46.3	0.67	0.59	0.71	33.38	40.71	29.41
					10	−10	103.8	99.6	95.0	105.6	0.96	0.91	1.02	4.06	8.54	1.71
					100	25	65.6	50.9	47.4	56.0	0.78	0.72	0.85	22.49	27.86	14.62
					100	−25	71.6	52.5	47.9	57.7	0.73	0.67	0.81	26.71	33.06	19.40
					200	50	40.0	31.7	30.4	34.9	0.79	0.76	0.87	20.57	23.96	12.63
					200	−50	49.0	33.0	30.8	36.2	0.67	0.63	0.74	32.74	37.12	26.10
					0	10	263.3	295.0	301.6	302.2	1.12	1.15	1.15	12.02	14.54	14.77
					0	−10	279.8	307.5	304.9	314.3	1.10	1.09	1.12	9.88	8.95	12.32
					0	25	197.5	223.7	243.9	231.0	1.13	1.24	1.17	13.32	23.52	17.01
					0	−25	223.2	242.5	248.7	250.1	1.09	1.11	1.12	8.61	11.41	12.01
					0	50	148.1	159.5	188.5	164.8	1.08	1.27	1.11	7.75	27.28	11.30
					0	−50	170.8	179.3	193.9	185.3	1.05	1.14	1.08	4.96	13.53	8.48
					10	0	355.6	339.1	318.8	344.0	0.95	0.90	0.97	4.65	10.35	3.27
3000	200	4	81.7	50	100	0	237.3	183.3	162.2	189.4	0.77	0.68	0.80	22.75	31.64	20.16
					200	0	148.1	121.3	108.4	125.0	0.82	0.73	0.84	18.05	26.79	15.56
					10	10	263.4	272.6	263.5	282.3	1.03	1.00	1.07	3.48	0.02	7.16
					10	−10	277.8	283.2	266.0	292.7	1.02	0.96	1.05	1.95	4.26	5.37
					100	25	149.4	137.8	128.9	145.1	0.92	0.86	0.97	7.75	13.76	2.88
					100	−25	184.5	144.7	130.3	152.2	0.78	0.71	0.83	21.56	29.35	17.50
					200	50	94.8	84.5	81.4	88.8	0.89	0.86	0.94	10.86	14.14	6.29
					200	−50	120.9	89.7	82.5	94.2	0.74	0.68	0.78	25.82	31.78	22.07
					0	−10	22.8	22.2	23.1	24.9	0.98	1.01	1.09	2.43	1.34	9.30
					0	25	27.5	19.7	18.7	22.6	0.72	0.68	0.82	28.31	32.04	17.68
					0	−25	17.9	16.7	18.7	19.5	0.93	1.04	1.09	6.94	4.35	8.75
					0	50	16.5	15.0	14.5	17.7	0.91	0.88	1.07	8.76	12.33	7.02
					0	−50	13.4	11.8	14.5	13.7	0.88	1.08	1.03	12.19	7.94	2.56
					10	0	28.5	27.2	26.1	28.1	0.95	0.92	0.99	4.78	8.49	1.44
1500	300	1	83.4	300	100	0	24.9	18.8	16.8	21.7	0.76	0.67	0.87	24.49	32.54	12.70
					200	0	20.4	14.0	12.4	16.4	0.69	0.61	0.81	31.37	39.13	19.47
					10	−10	22.7	21.4	21.4	24.6	0.94	0.94	1.08	6.08	6.01	7.99
					100	25	21.3	14.5	12.6	18.3	0.68	0.59	0.86	31.84	40.84	13.89
					100	−25	16.5	12.8	12.6	16.3	0.77	0.76	0.99	22.67	23.85	1.37
					200	50	12.6	9.7	8.4	12.5	0.77	0.67	1.00	22.63	32.71	0.37
					200	−50	11.5	8.2	8.4	10.6	0.72	0.74	0.92	28.34	26.44	8.03
					0	−10	63.9	67.1	65.4	71.3	1.05	1.02	1.12	4.99	2.28	11.56
					0	25	57.3	43.6	50.2	47.8	0.76	0.88	0.83	23.80	12.26	16.61
					0	−25	49.1	52.2	51.9	56.8	1.06	1.06	1.16	6.24	5.79	15.71
					0	50	37.7	29.6	37.6	32.2	0.78	1.00	0.85	21.59	0.31	14.70
					0	−50	35.4	38.0	39.4	41.6	1.07	1.11	1.17	7.37	11.34	17.46
					10	0	82.9	80.5	78.1	81.7	0.97	0.94	0.99	2.91	5.76	1.46
1500	300	2	85.4	150	100	0	72.9	63.1	57.1	67.6	0.87	0.78	0.93	13.44	21.72	7.21
					200	0	59.5	50.9	45.2	55.5	0.85	0.76	0.93	14.51	24.05	6.78
					10	−10	63.8	65.5	62.2	70.4	1.03	0.97	1.10	2.54	2.54	10.22
					100	25	53.8	37.4	38.8	42.6	0.70	0.72	0.79	30.43	27.81	20.82
					100	−25	45.9	43.5	39.9	49.5	0.95	0.87	1.08	5.19	13.14	7.82
					200	50	33.3	24.2	26.5	27.5	0.72	0.80	0.83	27.53	20.37	17.48

(*continued on next page*)

Table A.2 (*continued*).

					200	−50	31.1	29.5	27.5	33.9	0.95	0.88	1.09	5.17	11.64	8.93
					0	10	160.8	160.3	154.5	167.1	1.00	0.96	1.04	0.30	3.91	3.90
					0	−10	153.5	160.9	157.6	167.6	1.05	1.03	1.09	4.83	2.68	9.23
					0	25	106.2	112.2	111.4	117.8	1.06	1.05	1.11	5.68	4.91	10.92
					0	−25	110.5	112.9	115.1	118.5	1.02	1.04	1.07	2.21	4.19	7.27
					0	50	71.5	74.8	77.6	78.2	1.05	1.08	1.09	4.59	8.46	9.31
					0	−50	76.0	75.4	81.0	78.8	0.99	1.07	1.04	0.75	6.62	3.74
					10	0	209.7	214.2	206.1	216.8	1.02	0.98	1.03	2.18	1.71	3.40
1500	300	4	89.8	75	100	0	186.2	152.1	135.9	158.8	0.82	0.73	0.85	18.34	27.02	14.70
					200	0	152.2	115.0	101.8	120.7	0.76	0.67	0.79	24.44	33.11	20.69
					10	10	160.6	155.0	145.1	162.9	0.97	0.90	1.01	3.49	9.67	1.40
					10	−10	153.3	155.6	147.8	163.4	1.01	0.96	1.07	1.48	3.55	6.60
					100	25	100.6	90.6	82.3	97.5	0.90	0.82	0.97	9.86	18.13	3.03
					100	−25	105.6	91.1	84.4	98.0	0.86	0.80	0.93	13.70	20.02	7.16
					200	50	64.2	56.8	52.7	61.0	0.88	0.82	0.95	11.54	17.86	4.95
					200	−50	69.9	57.1	54.4	61.4	0.82	0.78	0.88	18.25	22.18	12.14
					0	−10	23.4	23.9	23.8	25.6	1.02	1.02	1.09	2.28	1.85	9.38
					0	25	27.2	17.4	20.0	19.8	0.64	0.73	0.73	36.12	26.65	27.28
					0	−25	19.6	20.1	20.6	22.4	1.02	1.05	1.15	2.49	4.96	14.56
					0	50	20.7	12.7	16.3	14.6	0.62	0.79	0.71	38.36	21.20	29.24
					0	−50	15.7	15.8	17.0	18.1	1.01	1.08	1.16	0.93	8.46	15.58
					10	0	27.3	25.9	24.8	26.8	0.95	0.91	0.98	5.29	9.34	2.00
3000	250	1	106.7	250	100	0	23.3	17.3	15.4	19.7	0.74	0.66	0.84	25.86	34.03	15.57
					200	0	18.3	12.6	11.2	14.5	0.69	0.61	0.79	30.90	38.83	20.69
					10	−10	23.3	22.8	21.8	25.0	0.98	0.93	1.07	2.43	6.66	7.40
					100	25	20.0	12.7	12.6	15.7	0.64	0.63	0.78	36.43	37.10	21.53
					100	−25	17.4	14.1	12.8	17.2	0.81	0.74	0.99	19.09	26.34	1.22
					200	50	13.6	8.3	8.5	10.3	0.61	0.63	0.76	39.25	37.25	24.36
					200	−50	12.4	9.5	8.8	11.7	0.77	0.71	0.95	23.40	29.15	5.00
					0	−10	63.8	65.5	65.5	68.4	1.03	1.03	1.07	2.71	2.69	7.13
					0	25	65.2	54.4	55.1	58.1	0.84	0.85	0.89	16.44	15.44	10.81
					0	−25	53.1	54.2	56.1	57.9	1.02	1.06	1.09	2.14	5.70	9.05
					0	50	47.0	42.4	44.8	45.7	0.90	0.95	0.97	9.91	4.80	2.78
					0	−50	42.0	42.1	46.1	45.5	1.00	1.10	1.08	0.34	9.72	8.29
					10	0	76.0	74.0	71.9	74.9	0.97	0.95	0.99	2.61	5.32	1.42
3000	250	2	108.4	125	100	0	67.2	59.0	53.5	62.5	0.88	0.80	0.93	12.11	20.32	6.92
					200	0	54.8	48.2	42.9	51.9	0.88	0.78	0.95	12.04	21.78	5.43
					10	−10	63.7	64.0	62.3	67.4	1.00	0.98	1.06	0.42	2.11	5.80
					100	25	52.9	45.1	41.8	50.1	0.85	0.79	0.95	14.64	20.93	5.29
					100	−25	48.4	45.0	42.4	49.9	0.93	0.88	1.03	7.03	12.33	3.17
					200	50	34.8	32.1	30.1	36.1	0.92	0.87	1.04	7.76	13.29	3.90
					200	−50	34.9	31.9	30.8	36.0	0.92	0.88	1.03	8.44	11.78	3.14
					0	10	168.4	160.7	159.7	164.7	0.95	0.95	0.98	4.53	5.14	2.17
					0	−10	156.3	161.8	161.4	165.7	1.04	1.03	1.06	3.51	3.25	6.01
					0	25	124.3	130.9	134.2	135.7	1.05	1.08	1.09	5.31	7.95	9.18
					0	−25	126.1	132.7	136.9	137.5	1.05	1.09	1.09	5.22	8.54	9.04
					0	50	92.4	100.0	107.9	104.1	1.08	1.17	1.13	8.26	16.79	12.76
					0	−50	96.7	102.1	111.1	106.3	1.06	1.15	1.10	5.56	14.91	9.93
					10	0	189.3	181.4	174.8	183.2	0.96	0.92	0.97	4.17	7.69	3.23
3000	250	4	112.0	63	100	0	167.3	131.0	117.2	135.8	0.78	0.70	0.81	21.68	29.93	18.80

(*continued on next page*)

Table A.2 (*continued*).

					200	0	133.1	100.1	88.6	104.3	0.75	0.67	0.78	24.79	33.47	21.67
					10	10	167.7	154.9	148.9	159.9	0.92	0.89	0.95	7.66	11.24	4.63
					10	−10	156.0	155.9	150.3	160.9	1.00	0.96	1.03	0.10	3.64	3.11
					100	25	107.6	100.0	92.2	106.2	0.93	0.86	0.99	7.06	14.38	1.35
					100	−25	117.0	101.1	93.5	107.3	0.86	0.80	0.92	13.59	20.07	8.31
					200	50	71.4	68.0	63.8	72.5	0.95	0.89	1.02	4.75	10.62	1.60
					200	−50	82.0	68.9	65.0	73.5	0.84	0.79	0.90	15.98	20.77	10.38
					0	−10	12.0	12.4	12.3	13.2	1.03	1.03	1.10	3.35	2.88	10.42
					0	25	15.2	9.7	10.8	11.1	0.64	0.71	0.73	35.95	28.54	26.63
					0	−25	10.2	10.7	10.8	12.0	1.04	1.06	1.17	4.17	5.94	17.06
					0	50	10.8	7.5	9.2	8.8	0.69	0.85	0.81	30.97	15.36	19.07
					0	−50	8.4	8.6	9.2	10.1	1.03	1.09	1.20	3.13	9.22	19.91
					10	0	13.9	13.5	13.2	13.8	0.98	0.95	0.99	2.46	4.70	0.60
3000	300	1	166.8	300	100	0	13.1	11.0	10.1	12.3	0.84	0.77	0.94	15.85	23.15	6.30
					200	0	11.7	9.1	8.2	10.6	0.78	0.70	0.90	21.96	30.19	9.82
					10	−10	12.0	12.1	11.8	13.1	1.01	0.98	1.10	1.05	1.76	9.76
					100	25	14.0	8.2	8.3	10.1	0.59	0.59	0.73	41.12	40.64	27.46
					100	−25	9.7	8.9	8.3	10.8	0.92	0.86	1.12	8.27	14.47	11.51
					200	50	8.6	5.8	6.2	7.5	0.68	0.71	0.86	32.30	28.54	13.65
					200	−50	7.4	6.5	6.2	8.3	0.89	0.84	1.13	11.02	16.11	13.19
					0	−10	30.7	31.6	31.7	33.0	1.03	1.03	1.08	2.98	3.18	7.56
					0	25	19.0	25.9	27.3	27.9	1.36	1.43	1.47	36.16	43.46	46.81
					0	−25	25.8	26.9	27.8	28.8	1.04	1.08	1.12	4.28	7.98	11.98
					0	50	22.8	20.3	22.8	22.1	0.89	1.00	0.97	11.22	0.21	2.94
					0	−50	20.6	21.5	23.5	23.4	1.04	1.14	1.14	4.42	14.12	13.96
					10	0	35.8	34.9	33.9	35.3	0.97	0.95	0.99	2.65	5.34	1.33
3000	300	2	170.8	150	100	0	34.0	28.0	25.5	29.9	0.82	0.75	0.88	17.61	25.16	12.01
					200	0	30.1	23.0	20.5	25.0	0.76	0.68	0.83	23.53	31.86	16.81
					10	−10	30.7	30.8	30.1	32.6	1.01	0.98	1.06	0.57	1.72	6.26
					100	25	28.1	21.5	20.6	24.3	0.77	0.74	0.87	23.25	26.45	13.44
					100	−25	24.8	22.2	21.0	25.0	0.89	0.84	1.01	10.56	15.58	0.60
					200	50	19.2	15.4	15.2	17.7	0.80	0.79	0.92	19.92	21.16	7.96
					200	−50	18.8	16.1	15.5	18.5	0.86	0.82	0.98	14.39	17.60	1.66
					0	10	72.8	68.7	65.3	70.3	0.94	0.90	0.97	5.65	10.30	3.48
					0	−10	65.0	67.3	65.9	69.1	1.04	1.01	1.06	3.58	1.40	6.23
					0	25	56.5	59.1	55.2	61.4	1.05	0.98	1.09	4.55	2.45	8.51
					0	−25	53.5	56.7	56.2	59.0	1.06	1.05	1.10	5.90	4.94	10.20
					0	50	42.7	48.0	44.6	50.2	1.12	1.04	1.18	12.39	4.44	17.68
					0	−50	42.0	44.8	45.8	47.0	1.07	1.09	1.12	6.67	8.98	11.84
					10	0	77.0	75.1	73.3	75.7	0.98	0.95	0.98	2.37	4.77	1.67
3000	300	4	179.6	75	100	0	73.1	61.8	56.4	63.9	0.85	0.77	0.87	15.47	22.88	12.56
					200	0	64.9	51.6	46.1	53.9	0.80	0.71	0.83	20.46	28.97	16.89
					10	10	72.6	67.2	62.5	69.2	0.93	0.86	0.95	7.47	13.89	4.75
					10	−10	65.0	65.9	63.1	68.0	1.01	0.97	1.05	1.45	2.85	4.68
					100	25	52.1	49.7	43.3	52.9	0.95	0.83	1.02	4.51	16.86	1.53
					100	−25	52.1	48.0	43.9	51.1	0.92	0.84	0.98	7.86	15.65	1.86
					200	50	35.8	36.7	31.5	39.5	1.03	0.88	1.10	2.50	12.10	10.28
					200	−50	39.2	34.9	32.1	37.5	0.89	0.82	0.96	11.04	17.99	4.24
					Average						**0.91**	**0.89**	**0.99**	**12.38**	**15.55**	**9.80**

Table A.3
Comparison between the strength of CFS beam–columns with NZ standard cross-sections obtained using FE analysis (P_{FE}), code-prescribed linear interaction equation (P_{Code}) and proposed interaction equation (P_{Prop}).

Length	Web height	Thickness	Element slenderness ratio	Web slenderness ratio	Eccentricities		Capacity				
L (mm)	h (mm)	t (mm)	λ_y	h/t	e_y (mm)	e_x (mm)	P_{FE} (kN)	P_{Code} (kN)	P_{Prop} (kN)	$\frac{P_{Code}}{P_{FE}}$	$\frac{P_{Prop}}{P_{FE}}$
1500	152	0.75	63.7	203	0	10	29.1	19.8	21.2	0.68	0.73
					0	−10	18.9	18.2	19.8	0.96	1.05
					0	25	14.2	16.0	17.8	1.13	1.25
					0	−25	14.9	13.6	15.3	0.91	1.03
					0	50	9.1	12.2	13.7	1.33	1.50
					0	−50	11.2	9.6	10.7	0.86	0.96
					10	0	22.8	21.1	22.1	0.92	0.97
					100	0	13.8	10.9	12.3	0.79	0.89
					200	0	8.8	7.1	7.9	0.81	0.89
					10	10	25.8	18.0	20.1	0.70	0.78
					10	−10	18.5	16.7	18.9	0.90	1.02
					100	25	9.3	9.0	10.7	0.96	1.15
					100	−25	11.0	8.2	9.8	0.74	0.89
					200	50	5.5	5.5	6.6	1.01	1.19
					200	−50	7.0	4.9	5.9	0.70	0.84
1500	152	0.95	64.0	160	0	10	46.7	26.7	28.8	0.57	0.62
					0	−10	28.2	25.0	27.1	0.89	0.96
					0	25	21.5	19.4	21.4	0.90	0.99
					0	−25	22.1	17.3	19.0	0.78	0.86
					0	50	13.9	13.4	14.6	0.96	1.06
					0	−50	16.6	11.4	12.4	0.69	0.75
					10	0	34.8	33.1	34.1	0.95	0.98
					100	0	21.7	20.6	22.6	0.95	1.04
					200	0	13.9	14.5	15.9	1.04	1.14
					10	10	37.6	25.3	27.9	0.67	0.74
					10	−10	27.8	23.8	26.3	0.86	0.95
					100	25	14.7	13.9	16.1	0.95	1.10
					100	−25	16.8	12.8	14.8	0.76	0.88
					200	50	8.7	8.6	10.0	1.00	1.15
					200	−50	10.8	7.8	9.0	0.72	0.83
1500	152	1.15	64.2	132	0	10	41.2	38.9	41.7	0.94	1.01
					0	−10	48.0	41.9	44.6	0.87	0.93
					0	25	30.4	27.0	29.2	0.89	0.96
					0	−25	41.7	30.8	33.3	0.74	0.80
					0	50	21.2	17.9	19.2	0.84	0.90
					0	−50	35.2	21.3	23.1	0.61	0.65
					10	0	55.0	51.0	52.4	0.93	0.95
					100	0	43.8	30.3	32.9	0.69	0.75
					200	0	21.6	20.9	22.6	0.97	1.04
					10	10	40.5	36.8	40.2	0.91	0.99
					10	−10	47.9	39.4	42.8	0.82	0.90
					100	25	43.9	19.3	21.9	0.44	0.50
					100	−25	35.8	21.1	24.0	0.59	0.67
					200	50	13.8	11.7	13.2	0.84	0.95
					200	−50	25.2	13.1	14.8	0.52	0.59

(*continued on next page*)

Table A.3 (*continued*).

					0	10	11.1	9.8	10.3	0.88	0.93
					0	−10	9.4	9.5	10.0	1.01	1.07
					0	25	7.7	7.6	8.2	0.99	1.06
					0	−25	7.3	7.1	7.7	0.97	1.05
					0	50	5.3	5.6	6.0	1.06	1.14
					0	−50	5.5	5.1	5.4	0.92	0.99
					10	0	12.0	11.3	11.5	0.93	0.96
1500	89	0.75	100.2	119	100	0	8.4	7.0	7.5	0.84	0.90
					200	0	5.3	4.9	5.3	0.93	1.00
					10	10	10.7	9.3	9.9	0.86	0.92
					10	−10	9.3	9.0	9.6	0.96	1.04
					100	25	5.0	5.2	5.9	1.05	1.18
					100	−25	5.7	5.0	5.6	0.88	0.99
					200	50	2.9	3.3	3.8	1.17	1.31
					200	−50	3.6	3.2	3.5	0.88	0.99
					0	10	15.2	13.5	14.0	0.88	0.92
					0	−10	12.9	13.2	13.8	1.03	1.07
					0	25	10.9	10.4	11.1	0.96	1.02
					0	−25	10.1	10.1	10.7	1.00	1.06
					0	50	7.8	7.6	8.1	0.98	1.04
					0	−50	7.5	7.2	7.7	0.96	1.02
					10	0	16.7	15.2	15.6	0.92	0.94
1500	89	0.95	100.9	94	100	0	12.1	8.6	9.2	0.71	0.76
					200	0	8.2	5.8	6.2	0.71	0.75
					10	10	14.5	12.5	13.3	0.86	0.91
					10	−10	12.8	12.3	13.1	0.96	1.02
					100	25	7.0	6.6	7.2	0.94	1.03
					100	−25	7.9	6.5	7.1	0.82	0.90
					200	50	4.1	4.1	4.5	1.01	1.11
					200	−50	5.0	4.0	4.4	0.80	0.88
					0	10	18.7	18.2	18.7	0.98	1.00
					0	−10	16.5	18.4	18.9	1.12	1.15
					0	25	13.3	14.8	15.4	1.11	1.16
					0	−25	12.9	15.1	15.8	1.17	1.22
					0	50	9.3	11.2	11.8	1.21	1.27
					0	−50	9.5	11.6	12.2	1.22	1.28
					10	0	21.6	19.7	20.1	0.91	0.93
1500	89	1.15	101.6	77	100	0	15.9	11.2	11.8	0.70	0.74
					200	0	10.7	7.6	7.9	0.71	0.74
					10	10	17.8	16.9	17.7	0.95	0.99
					10	−10	16.4	17.0	17.8	1.04	1.09
					100	25	8.8	9.0	9.7	1.03	1.11
					100	−25	10.2	9.2	9.9	0.90	0.97
					200	50	5.1	5.7	6.2	1.11	1.20
					200	−50	6.4	5.8	6.3	0.91	0.98
					0	10	12.7	10.7	11.3	0.84	0.89
					0	−10	10.5	9.9	10.7	0.94	1.02
					0	25	8.6	9.1	10.0	1.05	1.16
					0	−25	9.0	7.7	8.6	0.86	0.96
					0	50	7.4	7.3	8.1	0.98	1.10

(*continued on next page*)

Table A.3 (*continued*).

					0	−50	7.3	5.7	6.4	0.77	0.87
					10	0	12.2	11.3	11.7	0.93	0.96
3000	152	0.75	127.4	203	100	0	9.9	7.0	7.8	0.70	0.79
					200	0	7.3	4.9	5.4	0.67	0.75
					10	10	12.4	10.1	11.0	0.81	0.88
					10	−10	10.5	9.3	10.4	0.89	0.99
					100	25	6.2	5.8	6.9	0.94	1.11
					100	−25	7.6	5.2	6.3	0.69	0.83
					200	50	3.7	3.8	4.6	1.03	1.22
					200	−50	5.2	3.3	4.0	0.64	0.77
					0	10	17.8	14.7	15.5	0.83	0.87
					0	−10	14.8	13.5	14.5	0.91	0.98
					0	25	12.8	12.1	13.1	0.95	1.03
					0	−25	12.7	10.3	11.3	0.81	0.89
					0	50	10.8	9.4	10.3	0.87	0.96
					0	−50	10.4	7.4	8.1	0.71	0.78
					10	0	17.1	16.0	16.5	0.94	0.96
3000	152	0.95	128.0	160	100	0	14.4	10.2	11.2	0.71	0.78
					200	0	10.8	7.3	8.0	0.68	0.74
					10	10	17.4	13.9	15.0	0.80	0.86
					10	−10	14.8	12.9	14.1	0.87	0.95
					100	25	9.4	8.2	9.5	0.88	1.01
					100	−25	10.9	7.3	8.5	0.67	0.78
					200	50	5.7	5.4	6.3	0.95	1.10
					200	−50	7.6	4.7	5.4	0.62	0.72
					0	10	23.6	18.8	19.8	0.80	0.84
					0	−10	19.9	19.6	20.4	0.98	1.03
					0	25	22.5	15.1	16.2	0.67	0.72
					0	−25	18.0	16.4	17.5	0.91	0.97
					0	50	14.7	11.3	12.3	0.77	0.83
					0	−50	16.2	12.9	13.9	0.80	0.86
					10	0	22.6	21.4	21.8	0.95	0.97
3000	152	1.15	128.5	132	100	0	19.3	14.6	15.8	0.76	0.82
					200	0	14.8	10.8	11.7	0.73	0.79
					10	10	23.1	18.0	19.2	0.78	0.83
					10	−10	19.9	18.7	19.9	0.94	1.00
					100	25	13.0	11.1	12.5	0.85	0.96
					100	−25	12.2	11.8	13.2	0.96	1.08
					200	50	8.0	7.3	8.3	0.92	1.04
					200	−50	12.2	8.0	9.0	0.65	0.74
					0	10	4.6	4.2	4.3	0.91	0.94
					0	−10	3.8	3.9	4.1	1.04	1.09
					0	25	3.9	3.6	3.8	0.94	0.99
					0	−25	3.3	3.2	3.4	0.96	1.02
					0	50	3.1	3.0	3.2	0.98	1.04
					0	−50	2.8	2.4	2.6	0.86	0.93
					10	0	4.7	4.4	4.5	0.94	0.96
3000	89	0.75	200.4	119	100	0	3.3	3.0	3.3	0.92	0.98

(*continued on next page*)

Table A.3 (*continued*).

					200	0	2.1	2.3	2.4	1.07	1.15
					10	10	4.4	4.0	4.2	0.91	0.95
					10	−10	3.8	3.8	4.0	1.00	1.06
					100	25	2.3	2.6	2.9	1.11	1.23
					100	−25	2.8	2.4	2.6	0.85	0.95
					200	50	1.4	1.8	2.0	1.25	1.40
					200	−50	1.9	1.6	1.8	0.82	0.92
3000	89	0.95	201.8	94	0	10	5.9	5.4	5.6	0.92	0.94
					0	−10	5.1	5.2	5.4	1.03	1.07
					0	25	5.1	4.6	4.8	0.91	0.95
					0	−25	4.5	4.3	4.5	0.96	1.01
					0	50	2.6	3.7	3.9	1.39	1.47
					0	−50	3.8	3.3	3.5	0.86	0.91
					10	0	6.2	5.9	6.0	0.95	0.96
					100	0	4.1	4.2	4.4	1.01	1.06
					200	0	2.7	3.1	3.3	1.18	1.26
					10	10	5.6	5.2	5.4	0.93	0.97
					10	−10	5.1	5.0	5.3	1.00	1.04
					100	25	3.0	3.4	3.7	1.13	1.23
					100	−25	3.8	3.2	3.5	0.86	0.93
					200	50	1.9	2.3	2.6	1.26	1.38
					200	−50	2.6	2.2	2.4	0.82	0.90
3000	89	1.15	203.1	77	0	10	7.1	6.8	7.0	0.96	0.98
					0	−10	6.4	6.6	6.8	1.04	1.07
					0	25	6.1	6.0	6.2	0.98	1.02
					0	−25	5.6	5.6	5.8	1.00	1.04
					0	50	5.0	4.9	5.1	0.99	1.03
					0	−50	4.8	4.4	4.7	0.93	0.98
					10	0	7.6	7.2	7.3	0.95	0.96
					100	0	5.0	5.2	5.4	1.04	1.09
					200	0	3.2	3.9	4.1	1.23	1.29
					10	10	6.7	6.5	6.8	0.98	1.01
					10	−10	6.4	6.4	6.6	1.00	1.04
					100	25	3.6	4.4	4.7	1.20	1.29
					100	−25	4.7	4.2	4.5	0.88	0.94
					200	50	2.3	3.1	3.3	1.36	1.46
					200	−50	3.4	2.9	3.1	0.86	0.93

References

[1] Daniel P. McCrum, Jordan Simon, Michael Grimes, Brian M. Broderick, James B.P. Lim, Andrzej M. Wrzesien, Experimental cyclic performance of cold-formed steel bolted moment resisting frames, Eng. Struct. 181 (2019) 1–14, http://dx.doi.org/10.1016/j.engstruct.2018.11.063.

[2] Seyed Mohammad Mojtabaei, Mohammad Zaman Kabir, Iman Hajirasouliha, Mina Kargar, Analytical and experimental study on the seismic performance of cold-formed steel frames, J. Construct. Steel Res. 143 (2018) 18–31, http://dx.doi.org/10.1016/j.jcsr.2017.12.013.

[3] Duoc T. Phan, Seyed Mohammad Mojtabaei, Iman Hajirasouliha, Jun Ye, James B.P. Lim, Coupled element and structural level optimisation framework for cold-formed steel frames, J. Construct. Steel Res. 168 (2020) 105867, http://dx.doi.org/10.1016/j.jcsr.2019.105867.

[4] Seyed Mohammad Mojtabaei, Jurgen Becque, Iman Hajirasouliha, Structural size optimization of single and built-up cold-formed steel beam-column members, J. Struct. Eng. 147 (4) (2021) 04021030, http://dx.doi.org/10.1061/(ASCE)ST.1943-541X.0002987.

[5] Ioannis Papargyriou, Iman Hajirasouliha, More efficient design of CFS strap-braced frames under vertical and seismic loading, J. Construct. Steel Res. 185 (2021) 106886, http://dx.doi.org/10.1016/j.jcsr.2021.106886.

[6] Fatih Yilmaz, Seyed Mohammad Mojtabaei, Iman Hajirasouliha, Jurgen Becque, Behaviour and performance of OSB-sheathed cold-formed steel stud wall panels under combined vertical and seismic loading, Thin-Walled Struct. 183 (2023) 110419, http://dx.doi.org/10.1016/j.tws.2022.110419.

[7] Seyed Mohammad Mojtabaei, Jurgen Becque, Iman Hajirasouliha, Local buckling in cold-formed steel moment-resisting bolted connections: behavior, capacity, and design, J. Struct. Eng. 146 (9) (2020) 04020167, http://dx.doi.org/10.1061/(ASCE)ST.1943-541X.0002730.

[8] Seyed Mohammad Mojtabaei, Jurgen Becque, Iman Hajirasouliha, Behavior and design of cold-formed steel bolted connections subjected to combined actions, J. Struct. Eng. 147 (4) (2021) 04021013, http://dx.doi.org/10.1061/(ASCE)ST.1943-541X.0002966.

[9] Shahabeddin Torabian, Baofeng Zheng, Benjamin W. Schafer, Experimental response of cold-formed steel lipped channel beam–columns, Thin-Walled Struct. 89 (2015) 152–168, http://dx.doi.org/10.1016/j.tws.2014.12.003.

[10] Shahabeddin Torabian, David C. Fratamico, Benjamin W. Schafer, Experimental response of cold-formed steel Zee-section beam–columns, Thin-Walled Struct. 98 (2016) 496–517, http://dx.doi.org/10.1016/j.tws.2015.10.016.

[11] AISI (American Iron and Steel Institute), North American Specification for the Design of Cold-Formed Steel Structural Members, AISI S100-12, AISI, Washington, DC, 2012.

[12] Yuanqi Li, Yinglei Li, Yanyong Song, Experimental investigation on ultimate capacity of eccentrically-compressed cold-formed beam–columns with lipped channel sections, in: Paper presented at 22^{n}d International Specialty Conference on Cold-Formed Steel Structures, St. Loius, 2014, https://scholarsmine.mst.edu/isccss/22iccfss/session04/3.

[13] G.J. Hancock, K.J.R. Rasmussen, Recent research on thin-walled beam–columns, Thin-Walled Struct. 32 (1–3) (1998) 3–18, http://dx.doi.org/10.1016/S0263-8231(98)00025-1.

[14] Shan-shan Cheng, Boksun Kim, Long-yuan Li, Lateral–torsional buckling of cold-formed channel sections subject to combined compression and bending, J. Construct. Steel Res. 80 (2013) 174–180, http://dx.doi.org/10.1016/j.jcsr.2012.07.026.

[15] Jia-Lin Ma, Tak-Mings Chan, Ben Young, Cold-formed high-strength steel rectangular and square hollow sections under combined compression and bending, J. Struct. Eng. 145 (12) (2019) 04019154, http://dx.doi.org/10.1061/(ASCE)ST.1943-541X.0002446.

[16] ANSI/AISC (American National Standards Institute of steel Construction), Specification for Structural Steel Buildings, ANSI/AISC 360-10, AISC, Chicago, 2010.

[17] CEN (European Committee for Standardization), Eurocode 3: Design of Steel Structures—Part 1–1: General Rules and Rules for Buildings, CEN, Brussels, Belgium, 2005.

[18] AS (Australia Standards), Standards Australia International, AS, New South Wales, Australia, 1990.

[19] Qiu-Yun Li, Ben Young, Tests of cold-formed steel built-up open section members under eccentric compressive load, J. Construct. Steel Res. 184 (2021) 106775, http://dx.doi.org/10.1016/j.jcsr.2021.106775.

[20] AISI (American Iron and Steel Institute), North American Specification for the Design of Cold-Formed Steel Structural Members (AISI S100-16), AISI, Washington, DC, 2016.

[21] AS/NZS 4600 (Australian Standard/New Zealand Standard), Cold-formed steel structures. Sydney/Wellington, 2018.

[22] ANSI/AISC (American National Standards Institute of steel Construction), Specification for Structural Steel Buildings, ANSI/AISC 360-16, AISC, Chicago, 2016.

[23] Qiu-Yun Li, Ben Young, Design of cold-formed steel built-up open section members under combined compression and bending, Thin-Walled Struct. 172 (2022) 108890, http://dx.doi.org/10.1016/j.tws.2022.108890.

[24] Bin Wang, Guillaume L. Bosco, Benoit P. Gilbert, Hong Guan, Lip H. Teh, Unconstrained shape optimisation of singly-symmetric and open cold-formed steel beams and beam–columns, Thin-Walled Struct. 104 (2016) 54–61, http://dx.doi.org/10.1016/j.tws.2016.03.007.

[25] Hossein Parastesh, Seyed Mohammad Mojtabaei, Hamed Taji, Iman Hajirasouliha, Alireza Bagheri Sabbagh, Constrained optimization of anti-symmetric cold-formed steel beam–column sections, Eng. Struct. 228 (2021) 111452, http://dx.doi.org/10.1016/j.engstruct.2020.111452.

[26] Maryam Hasanali, Seyed Mohammad Mojtabaei, G. Charles Clifton, Iman Hajirasouliha, Shahabbeddin Torabian, James B.P. Lim, Capacity and design of cold-formed steel warping-restrained beam–columns, J. Construct. Steel Res. 190 (2022) 107139, http://dx.doi.org/10.1016/j.jcsr.2022.107139.

[27] Ferhan Öztürk, Seyed Mohammad Mojtabaei, Mehmet Şentürk, Selim Pul, Iman Hajirasouliha, Buckling behaviour of cold-formed steel sigma and lipped channel beam–column members, Thin-Walled Struct. 173 (2022) 108963, http://dx.doi.org/10.1016/j.tws.2022.108963.

[28] CEN (European Committee for Standardization), Eurocode 3: Design of steel structures-Part 1-3: General rules: Supplementary rules for cold-formed members and sheeting. Brussels, 2022.

[29] CEN (European Committee for Standardization), Eurocode 3: Design of steel structures-Part 1-1: General rules and rules for buildings. Brussels, 2020.

[30] CEN (European Committee for Standardization), Eurocode 3: Design of steel structures-Part 1-5: Plated structural elements. Brussels, 2020.

[31] Benjamin W. Schafer, Teoman Peköz, Direct strength prediction of cold-formed steel members using numerical elastic buckling solutions, 1998.

[32] Shahabeddin Torabian, Baofeng Zheng, B.W. Schafer, Direct Strength Prediction of Cold-Formed Steel Beam–Columns, Research Rep. RP16-3, American Iron and Steel Institute, Ithaca, NY, 2016.

[33] Abaqus/CAE User's Manual, version 6.23, USA, 2021.

[34] I. Papargyriou, S.M. Mojtabaei, I. Hajirasouliha, J. Becque, K. Pilakoutas, Cold-formed steel beam-to-column bolted connections for seismic applications, Thin-Walled Struct. 172 (2022) 108876, http://dx.doi.org/10.1016/j.tws.2021.108876.

[35] Seyed Mohammad Mojtabaei, Iman Hajirasouliha, Jun Ye, Optimisation of cold-formed steel beams for best seismic performance in bolted moment connections, J. Construct. Steel Res. 181 (2021) 106621, http://dx.doi.org/10.1016/j.jcsr.2021.106621.

[36] Benjamin William Schafer, Zhan Li, Cristopher Dennis Moen, Computational modelling of cold-formed steel, Thin-Walled Struct. 48 (10–11) (2010) 752–762, http://dx.doi.org/10.1016/j.tws.2010.04.008.

[37] Cheng Yu, Benjamin W. Schafer, Distortional buckling tests on cold-formed steel beams, J. Struct. Eng. 132 (4) (2006) 515–528, http://dx.doi.org/10.1061/(ASCE)0733-9445(2006)132:4(515).

[38] Benjamin W. Schafer, Teoman Peköz, Laterally braced cold-formed steel flexural members with edge stiffened flanges, J. Struct. Eng. 125 (2) (1999) 118–127, http://dx.doi.org/10.1061/(ASCE)0733-9445(1999)125:2(118).

[39] B. Schafer, CUFSM Version 5.04, Department of Civil Engineering, Johns Hopkins University, 2006, http://www.ce.jhu.edu/bschafer/cufsm/.

[40] Benjamin W. Schafer, Teoman Peköz, Computational modeling of cold-formed steel: characterizing geometric imperfections and residual stresses, J. Construct. Steel Res. 47 (3) (1998b) 193–210, http://dx.doi.org/10.1016/S0143-974X(98)00007-8.

[41] A.C. Walker (Ed.), Design and Analysis of Cold-Formed Sections, John Wiley & Sons, 1975.

[42] Jun Ye, Seyed Mohammad Mojtabaei, Iman Hajirasouliha, Local-flexural interactive buckling of standard and optimised cold-formed steel columns, J. Construct. Steel Res. 144 (2018) 106–118, http://dx.doi.org/10.1016/j.jcsr.2018.01.012.

[43] Francisco Meza Ortiz, The Behaviour of Cold-Formed Steel Built-Up Structural Members (PhD diss), The University of Sheffield, 2018.

[44] Yared Shifferaw, B.W. Schafer, Inelastic bending capacity of cold-formed steel members, J. Struct. Eng. 138 (4) (2012) 468–480, http://dx.doi.org/10.1061/(ASCE)ST.1943-541X.0000469.

[45] Ling-En Hsiao, Wei-Wen Yu, Theodore V. Galambos, AISI LRFD method for cold-formed steel structural members, J. Struct. Eng. 116 (2) (1990) 500–517, http://dx.doi.org/10.1061/(ASCE)0733-9445(1990)116:2(500).